UNIVERSITY OF CALIFORNIA
RIVERSIDE

On the Common Origin of Dark and Baryonic Matter Abundacnes and Cosmological Probes of the Dirac Neutrino

A Dissertation submitted in partial satisfaction
of the requirements for the degree of

Doctor of Philosophy

in

Physics

by

Michael Shamma

June 2021

Dissertation Committee:

Dr. Yanou Cui, Chairperson
Dr. Flip Tanedo
Dr. Hai-Bo Yu

The Dissertation of Michael Shamma is approved:

Committee Chairperson

University of California, Riverside

Acknowledgments

I have immense gratitude for my advisor, Dr. Yanou Cui, whose expertise, guidance, and patience made this thesis and the work contained possible. I am very grateful to the other members of this committee, Dr. Hai-Bo Yu and Dr. Flip Tanedo, for their support, instruction, and valuable advice in my time at UCR.

I give special thanks to Dr. Aniket Joglekar and Dr. Andrew J. Long for the knowledge passed to me in countless discussions on a variety of topics in particle physics and cosmology. I would also like to thank Ian Chaffey, Gerardo Alvarez, Chia-Feng Chang, and Lexi Constantino for many enlightening discussions on physics and beyond in my time as a student.

I would like to express love and thanks to my parents, sister, and Brittany Wightman. This accomplishment would not have been possible without their support. Special thanks are due to my best friends Ryan Schoenbaum and Jack Chellemi whose friendship and distracting support are invaluable.

In addition to work in progress, work that appears in this thesis is based on previously published work from [1, 2]. I thank and acknowledge the contribution of my co-authors to these published works.

ABSTRACT OF THE DISSERTATION

On the Common Origin of Dark and Baryonic Matter Abundacnes
and Cosmological Probes of the Dirac Neutrino

by

Michael Shamma

Doctor of Philosophy, Graduate Program in Physics
University of California, Riverside, June 2021
Dr. Yanou Cui, Chairperson

Although the Standard Model has been a successful description of observed particles and interactions, there exist open questions and observations which motivate physics beyond its framework. Of particular importance are the need for new particles and interactions to explain the origins of the baryon asymmetry, the nature of dark matter, and generation of neutrino mass. This work is motivated by the coincidental similarity between the baryon asymmetry and abundance of dark matter which, when taken together with their mysterious origins, constitutes a *cosmological triple puzzle*. In this thesis, unique mechanisms which propose new interactions and symmetries between quarks and dark matter candidates unambiguously address this triple puzzle. The first is a mechanism is a renormalizable model which produces the observed baryon asymmetry and an asymmetric dark matter (ADM) abundance simultaneously through the decays of a WIMP. A second mechanism is proposed which utilizes a multicomponent dark sector to relate the baryon asymmetry directly to the abundance of a symmetric dark matter candidate. These models predict interesting experimental signatures such as induced proton decay.

Additionally, work in thesis is driven by the need to explain neutrino masses. In particular, it is unknown whether neutrino masses are Majorana or Dirac. Observation of neutrino-less double beta decay would provide evidence of Majorana masses while observing Dirac masses is much more difficult to achieve. A number of new frameworks which generate neutrino masses such as gauged $U(1)_{B-L}$ and Dirac leptogenesis, utilize new interactions for neutrinos which would lead to measurable contributions to $N_{\rm eff}$ and $\sum m_\nu$ unique to Dirac neutrinos. Motivated by these imprints, this thesis also includes a new mechanism to test the Dirac nature of the neutrino by correlating variables used by cosmological and terrestrial probes.

Contents

List of Figures

List of Tables

Part I

Motivation

Chapter 1

Motivation

1.1 The Standard Model

The models presented in this thesis couple to the Standard Model (SM) of particle physics in various ways. The SM Lagrangian exhibits local gauge invariance under $SU(3)_C \times SU(2)_L \times U(1)_Y$ and has been remarkably successful at describing the interactions of three generations of quarks and leptons and a single scalar Higgs boson mediated by SM gauge bosons photons, gluons, and W and Z. These particles and their transformations under the SM gauge symmetry are shown in Table 1.1. The Higgs mechanism leads to the spontaneous symmetry breaking of $SU(2)_L$ and an explanation of the origin of the charged fermion, $W^{\pm}$, and Z boson masses.

The astounding success of the SM is not without its shortcomings. There are a number of observations which present challenges for the SM and require new physics to be appropriately explained. Searches for evidence of beyond the SM (BSM) physics has been

Particle	$SU(3)_C$	$SU(2)_L$	$U(1)_Y$
$Q_{i,L} = (u,d)_{i,L}$	**3**	**2**	$1/6$
$u_{i,R}$	**3**	**1**	$2/3$
$d_{i,R}$	**3**	**1**	$-1/3$
$L_{i,L} = (\nu,l)_{i,L}$	**1**	**2**	$-1/2$
$l_{i,R}$	**1**	**1**	-1
g	**8**	**1**	0
$W^{\pm}$	**1**	**3**	0
Z	**1**	**1**	0
γ	**1**	**1**	0
h	**1**	**2**	1

Table 1.1: Particle content and their representations in the Standard Model

taking place for over a decade at the LHC. However, no evidence of BSM physics has been observed with the statistical significance to warrant a "discovery" [10,11]. Although particle colliders have not, so far, provided the evidence of new physics astronomical, cosmological, and other terrestrial observations provide ample evidence of the necessity for BSM physics. These include the cosmological asymmetry of baryons over antibaryons [12], astrophysical and cosmological observations which require the existence of dark matter (DM) [13], and the observation of neutrino oscillations which require the neutrino to have nonzero mass [14].

Observations of cosmological abundances of DM and baryonic matter are coincidentally similar with $\Omega_{DM} \approx 5\Omega_B$ [15]. This similarity points to a physical mechanism connecting the two apparently distinct types of matter. That both the matter-antimatter asymmetry and DM abundance have mysterious origins and have similar cosmological densities is what we refer to as the *cosmological triple puzzle*. This similarity motivates work presented in Chapter 2 of this thesis which proposes models with unified production mechanisms for the abundances DM and baryons utilizing shared interactions and symmetries.

Additionally, new frameworks which generate Dirac neutrino masses such as gauged $U(1)_{B-L}$ and Dirac leptogenesis, utilize new interactions for neutrinos which would lead to a stronger cosmological imprint. Chapter 3 presents a mechanism to definitively test the Dirac nature of the neutrino by correlating these imprints with variables measured in terrestrial neutrino experiments.

1.2 The Matter-Antimatter Asymmetry

A triumph of the Big Bang Model of cosmology is its prediction of the relic abundances of the light elements such as hydrogen, helium, and lithium. The success of this process, referred to as Big Bang Nucleosynthesis (BBN), requires the initial condition of a small, but non-zero asymmetry of baryons over antibaryons [16]

$$\eta_B = \frac{n_B}{s} \simeq (5-7) \times 10^{-10} \tag{1.1}$$

This initial condition is referred to as the "baryon asymmetry of the universe" and is responsible for the relic asymmetry of matter over antimatter and the abundance of baryonic matter $\Omega_B h^2 \approx 0.0224$ [15]. It is possible for equal densities of matter and antimatter to be separated by widely distant regions in the universe. However, annihilation at the boundary separating regions of matter and antimatter would produce detectable gamma radiation and searches for these boundaries have made it very unlikely that any region of the observable universe is dominated by antimatter [17]. Alternatively, if the universe began with an initial baryon asymmetry, processes such as reheating would washout what is needed for BBN. Thus, some dynamical mechanism which produces this asymmetry, called *baryogenesis*, is needed to produce the initial condition for BBN and the baryon-antibaryon asymmetry.

In order to explain the origin of this initial condition, Sakharov proposed three conditions a model of baryogenesis must possess to be successful [18]. The first, and most straightforward, of these conditions is that baryon number must be violated. Quantum mechanically, this is easy to see in the Heisenberg picture where the time-evolution of baryon number B is determined by its commutation with the interaction Hamiltonian

$$\frac{dB}{dt} = -i[B, H_{\rm int}] \tag{1.2}$$

If interactions of a theory conserve baryon number, eigenstates of B are energy eigenstates and $[B, H] = 0$. In this case, the solution to Eq. 1.2 is constant. Thus, no baryon asymmetry can evolve without interactions which violate baryon number.

The second of these conditions is that the interactions of the model violate both charge (C) *and* combine charge-parity (CP) symmetries. The requirement that both be violated is simple to understand. Assume that baryon number and C are violated by the interactions of some set of fields but that CP is conserved. Thus, for a given helicity, the rate Γ^+ of a baryon number violating process which produces baryons is not equal to the rate of the charge-conjugate, antibaryon producing process Γ^-. However, when opposite helicity states are also taken into account, the rates of baryon and antibaryon producing processes satisfy $\Gamma^+_L + \Gamma^+_R = \Gamma^-_L + \Gamma^-_R$ because CP is a good symmetry and no net baryon number is produced. Thus to produce an asymmetry of baryons over antibaryons, interactions must violate both C and CP symmetries.

The third of these conditions is that the interactions of the model must depart from equilibrium. Because the combined symmetries of C, CP and time reversal (T) together should be conserved, the masses of baryons and antibaryons are the same. As the

production rate is weighted by a factor proportional to $\exp(-m/T)$ in equilibrium, baryon and antibaryon producing reactions are equally likely. So to produce a net baryon number, the interactions of the model must depart from equilibrium.

Within the SM, there are interactions which satisfy all three of these conditions. Global symmetries of baryon and lepton number permit anomalous baryon and lepton number violating currents $J^\mu_B = J^\mu_L \neq 0$ via locally gauge invariant, topologically stable field configurations, known as sphalerons. With three generations of quarks, there is a complex phase in the Cabibbo-Kobayashi-Maskawa (CKM) matrix which cannot be removed and leads to CP-violation, most notably in the neutral kaon system. The departure from equilibrium is accomplished by the electroweak phase transition (EWPT) that occurs as the universe cools and electroweak symmetry is broken. The SM mechanism to address the matter-antimatter asymmetry problem falls short because of insufficient baryon number violation, C/CP violation, and a smooth EWPT which allows sphalerons to washout any baryon asymmetry produced prior to the transition [19].

Beyond the SM, there are a few mechanisms for producing the baryon asymmetry [20, 21]. The mechanism seen in this thesis utilizes the baryon number violating decays of a heavy particle to SM quarks. The violation of C/CP is non-vanishing because of the interference of tree and one-loop Feynman diagrams which contribute to the total decay rate. The departure from equilibrium is achieved by an overabundant population of the particle decaying in an expanding universe.

1.3 Dark Matter

The evidence for Dark Matter (DM) stems from a number of astrophysical and cosmological sources. The sources include, but are not limited to: a mismatch between the observed velocity dispersions of stars in elliptical galaxies and the dispersions predicted by the virial theorem [22,23], its peculiar imprint on the cosmic microwave background (CMB) [15, 24], and the reliance of timely structure formation on the presence of DM [25]. There must also be an abundance of DM left after the cooling of the early universe to explain the observed DM density $\Omega_{DM}h^2 \approx 0.119$ [15]. To explain these observations, the essential traits a good DM candidate possesses include: gravitational interactions (i.e. is massive), exceedingly small or no electromagnetic charge, and stability (or a lifetime greater than the current age of the universe). Since the neutrino is the only SM particle which has these properties, it seemed plausible that it would make a good DM candidate. However, the neutrino decouples from the thermal bath of the early universe as a "hot relic", making it ill suited for use in the formation of large scale structure [26]. Thus to explain the abundance of DM, there must be physics beyond the SM.

A well motivated type of DM is a particle which has weak interactions or a mass and coupling strength similar to the weak scale. Usually stabilized through a discrete symmetry, such as Z_n, this class of DM is known as Weakly Interacting Massive Particle (WIMP) and have been a leading paradigm for DM model-building. These are particularly appealing because of what is referred to as the "WIMP miracle": through thermal freezeout of its annihilations, DM with weak-scale interactions and masses gives the correct DM abundance today. The WIMP paradigm does not address the DM-baryon coincidence triple puzzle as

mentioned in the previous section. Meanwhile, conventional WIMPs have been increasingly constrained by indirect/direct detection and collider experiments [27–29]. This has led to the proliferation of exploring alternative DM candidates beyond of the WIMP paradigm. Of particular interest in this thesis, in addition to the WIMP, is Asymmetric dark matter (ADM) [30–35] and Hidden (also Dark and Multicomponent) Sector models [36–38].

In most proposals, the explanation for DM and baryon abundances today are treated with separate mechanisms. The mysterious origins of both kinds of matter and their similar abundances together form the *cosmological triple puzzle* and suggests a physical connection between DM and baryons in the early Universe. In the ADM framework, the DM particle is distinct from its antiparticle, and an asymmetry in the particle-antiparticle number densities is generated in the early universe, much like the baryon asymmetry. The core idea of ADM is based on relating DM and baryons/leptons, through shared interactions in the early Universe as an explanation to their coincidentally similar abundances. The generation of the initial DM or baryon asymmetry for ADM often requires a separate baryogenesis-type of mechanism. Hidden sector DM constitutes particles whose interactions are mediated by other new particles. Additionally, interactions between hidden sector states and the SM may be extremely weak, indirect, mediated only through the gravitational interaction and/or via other new particles. Hidden sector models of DM are quite broad and can span a range of masses and interaction strengths but may include axions [39, 40], dark photon [37, 38], WIMP-like thermal relics [36, 41], and self-interacting DM [42–44].

In chapter 2, models connecting the baryon asymmetry to the relic abundance of dark matter are presented. The first relates the WIMP miracle to ADM and baryon

abundances and is based on work done in [1]. We also introduce a model which connects the baryon asymmetry to a symmetric, hidden, multicomponent sector DM and is based on work currently in progress.

1.4 Cosmological Consequences of Massive Neutrinos

The experimental detection of neutrino oscillations provides the evidence necessary to definitively claim that there must exist a non-zero mass difference between different flavors of neutrinos [14, 45, 46]. If it is assumed that both left and right-handed neutrinos exist, then the neutrino mass can be generated after electroweak symmetry breaking from interactions of the form $Y^{\nu}_{ij}\bar{L}^{i}\tilde{H}\nu^{j}_{R}$. Since L^{i} and $\tilde{H}$ have the same weak and hypercharge quantum numbers, the right-handed neutrino must have trivial weak and hypercharge quantum numbers and is referred to as "sterile". Because of this neutrality, the most general, renormalizable mass terms for the neutrino would also include a Majorana mass.

A variety of experimental efforts are currently underway to test the Majorana or Dirac nature of the neutrinos. The Majorana neutrino hypothesis (MNH) is particularly amenable to experimental probes, since these models generally predict lepton-number violation in two units, $\Delta L = \pm 2$, and thereby allow exotic nuclear reactions. For example, an observation of neutrinoless double beta decay [47] would validate the MNH and imply that neutrinos are their own antiparticles [48]. Confirmation of the Dirac neutrino hypothesis (DNH) is far harder to achieve because the DNH's new degrees of freedom are light gauge-singlet sterile neutrinos, which do not interact with the $W^{\pm}$ and Z bosons in the same way as the active neutrinos. Instead, their interactions are suppressed by the tiny Yukawa

coupling $y_\nu = m_\nu/v_{ew} = O(10^{-12})(m_\nu/0.1\text{ eV})$, making their production and detection in the lab exceedingly unlikely. These suppressed interactions would make not only terrestrial production of Dirac neutrinos unlikely, but also an undetectably small cosmological relic density.

New physics models that implement Dirac neutrinos generically introduce new fields and interactions that can efficiently thermalize the sterile neutrinos in the early universe [49–53]. This thermalization would enhance the production of Dirac neutrinos such that the cosmological relic population would be detectable through cosmological observables such as the effective neutrino mass sum $\sum m_\nu = m_{\text{active}} + m_{\text{sterile}}$ and the "effective number of neutrino species" N_{eff}, defined as the amount of relativistic energy density that is not in the form of cosmic microwave background (CMB) photons at decoupling measured in units of the energy carried by a SM neutrino. In the Λ-cold-dark-matter (ΛCDM) cosmology $N_{\text{eff}} = N_{\text{eff}}^{(0)} \simeq 3.044$ [54–58]. Provided that the sterile states were once in thermal equilibrium with the SM, the additional contribution to the radiation density is [59–62]

$$N_{\text{eff}} - N_{\text{eff}}^{(0)} \equiv \Delta N_{\text{eff}} \simeq (0.027 g_s)[106.75/g_*(T_{\text{dec}})]^{\frac{4}{3}} \tag{1.3}$$

where g_s is the effective number of degrees of freedom (d.o.f.) of the new species, which is $2 \times 3 \times 7/8 = 42/8$ in case of Dirac sterile neutrinos. T_{dec} is the temperature when the sterile states decouple, and $g_*(T_{\text{dec}})$ is the total effective number of d.o.f's in the thermal bath just above T_{dec}.

Chapter 3 of this thesis is based on work done in [2] where we point out that a combination of terrestrial neutrino mass measurements and cosmological probes ($\sum m_\nu$ and N_{eff}) of neutrinos can yield evidence in favor of the DNH.

Part II

Addressing the Cosmological Triple Puzzle

Chapter 2

WIMP Cogenesis for Asymmetric Dark Matter and the Baryon Asymmetry

2.1 Introduction

WIMP DM and ADM are both appealing proposals that address some aspect of the aforementioned cosmological triple puzzle about matter. However, it is intriguing to explore the possibility of a unified mechanism that combines their merits and addresses all three aspects of the puzzle simultaneously. Recently a few attempts have been made in this direction [63–70]. Among these existing proposals, [64] is highly sensitive to various initial conditions, while both [65] and WIMP DM annihilation triggered "WIMPy baryogensis" [63] have sensitivity to washout details. The mechanism of "Baryogenesis from Metastable WIMPs" [66] was then proposed as a alternative where the prediction is robust against model details: the baryon asymmetry is generated by a long-lived WIMP that undergoes CP- and B-violating decays after the thermal freezeout of the WIMP. Such models also provide a strong cosmological motivation for long-lived particle searches at the collider experiments and have become a benchmark for related studies [71–73]. However, the original model of Baryogenesis from Metastable WIMPs does not involve specifics of DM, only assuming that DM is another species of WIMP that is stable, and thus the DM-baryon coincidence is addressed by a generalized WIMP miracle which is not fully quantitative. From model building perspective it would be more desirable to further develop a framework which incorporates the merits of [66] as well as the details of DM, and predicts a tighter, more precise connection between $\Omega_{\rm DM}$ and Ω_B. There are two possible directions to pursue for this purpose: consider a WIMP DM that closely relates to the metastable baryon-parent WIMP in [66] (e.g. in the same multiplet or group representation), or consider a further deviation from [66] where the post-freezeout decay of a grandparent WIMP generates both

DM and baryon asymmetries, thus DM falls into the category of ADM. In this work we explore the latter possibility, which we naturally refer to as "WIMP cogenesis". The WIMP of our interest is of conventional weak scale mass or moderately higher (up to ~ 10 TeV). We aim at constructing a viable WIMP cogenesis model with the following guidelines:

- UV complete, only involves renormalizable interactions;
- ADM X and baryon asymmetries are generated in the same decay chain (instead of two different decay channels with potentially arbitrary branching ratios) so as to have the least ambiguity in predicting their "coincidence";
- The model possesses a generalized baryon/lepton number symmetry $U(1)_{B(L)+kX}$ that is conserved.

k is a model-dependent $O(1)$ rational number that parametrizes the ratio of ADM number to baryon (lepton) number produced in the decay chain. These first two guidelines distinguish our model from some other existing ADM proposals based on massive particle decay, such as [74–76]. In particular, the second guideline leads to a neat prediction of the ADM mass:

$$m_X = c_s \frac{1}{k} \frac{\Omega_X}{\Omega_B} m_n, \tag{2.1}$$

where $m_n \approx 1$ GeV is the neutron mass, $k = 2$ in the benchmark models we will demonstrate, the baryon distribution factor $c_s = \frac{n_B}{n_{B-L}} \sim O(1)$ depends on whether the EW sphaleron is active when the decays occur, and will be elaborated in Sec. 2.2.1. Given that $\frac{\Omega_X}{\Omega_B} \approx 5$ from observation, Eq. 2.1 generally predicts m_X in the GeV range. This possibility of producing DM and baryons in the same decay chain was suggested in the warped unification scenario

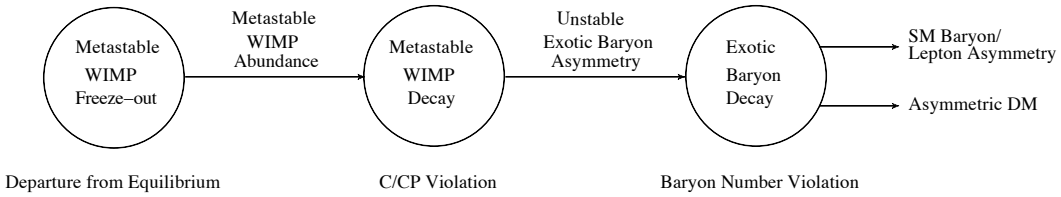

Figure 2.1: Schematic diagram outlining the key stages in WIMP cogenesis mechanism. Each dynamical stage of WIMP cogenesis, shown in the bubbles, satisfies one of the Sakharov conditions.

[77], while concrete examples remain to be seen. The third guideline, i.e., the idea of DM and baryon sharing a conserved global baryon number symmetry is also seen in e.g., [76, 78–80].

This new mechanism is illustrated in Fig. 2.1, which consists of three stages that satisfy each of the three Sakharov conditions in order.

1. Metastable WIMP freezeout. The out-of-equilibrium condition is automatically satisfied as a consequence of the WIMP freezeout. This step establishes a "would-be" WIMP miracle relic abundance predicted for the grandparent WIMP that will be inherited by Ω_X and Ω_B when the WIMP decays:

$$\begin{aligned} \Omega_B \sim \Omega_X &\approx \epsilon_{CP} \frac{m_{B(X)}}{m_{\rm WIMP}} \Omega_{\rm WIMP}^{\tau\to\infty} \\ &\approx 0.1 \epsilon_{CP} \frac{m_{B(X)}}{m_{\rm WIMP}} \frac{\alpha_{\rm weak}^2/({\rm TeV})^2}{\langle \sigma_{\rm ann,WIMP} v \rangle}. \end{aligned} \tag{2.2}$$

2. C- and CP-violating decay of the WIMP to intermediate states of exotic baryons/leptons. This occurs well after the freezeout and before BBN. The asymmetry between B and $\bar{B}$, or between DM and anti-DM originates from this stage.

3. Intermediate exotic baryons/leptons decay into SM baryons/leptons and ADM. This stage conserves the generalized $U(1)_{B(L)+X}$, the SM B-number symmetry is violated.

In the following sections, two models which accomplish this idea are presented and analyzed. The first of which produces the observed baryon asymmetry directly while the second first produces a lepton asymmetry which is converted to the observed abundance of baryons via sphaleron processes.

2.2 WIMP Decay to Baryons and ADM

In this section, we explore a specific model which directly produces a baryon asymmetry along with ADM via SM B-violating interactions. The fields and interactions are introduced followed by discussions on how Sakharov conditions are met by their interactions and the related cosmological evolution. This section ends with numerical analyses of the parameter space for these types of models.

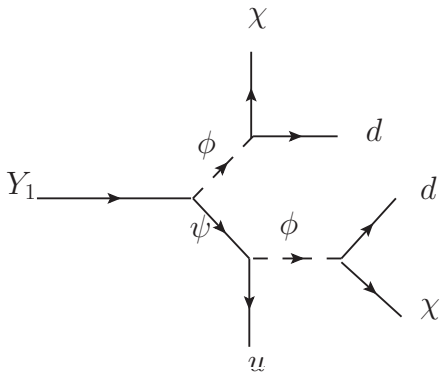

Figure 2.2: Feynman diagram of the WIMP decay chain producing baryon and DM asymmetries.

2.2.1 Model Setup

To implement the picture discussed in the introduction, we extend the SM with the following Lagrangian:

$$\begin{aligned}\mathcal{L} &= i\frac{1}{2}\bar{Y}_{1,2}\partial\!\!\!/ Y_{1,2} + \bar{\psi}_i(i\partial\!\!\!/ - m_\psi)\psi_i + \bar{\chi}(i\partial\!\!\!/ - m_\chi)\chi + (\partial^\mu\phi_i)^\dagger(\partial_\mu\phi_i) \\ &- m_\phi^2\phi^\dagger\phi - \eta_{1,2}\phi_i\bar{Y}_{1,2}P_R\psi_i - \alpha_{ii}\phi_i\bar{d}_iP_L\chi^c - \beta_{ijk}\phi_i\bar{\psi}_jP_Ru_k + \text{h.c.}\end{aligned} \tag{2.3}$$

where u^i and d^i are the SM quark fields. With the chiral projectors, only right-handed quarks are relevant. The SM singlet χ is the ADM, all Yukawa couplings are generic complex numbers, and β_{ijk} is anti-symmetric in its indices. Two Majorana fermions $Y_{1,2}$ are introduced: Y_1 plays the role of the WIMP grandparent for the ADM and baryon asymmetry, while Y_2 is essential for the interference process that enables C- and CP-violation (see Sec. 2.2.3). Three generations of diquark scalars ϕ_i and vector-like Dirac fermions ψ_i are the exotic baryons that are the intermediate decay products of metastable Y_1 as described in Stage-2 in Sec.2.1. This Lagrangian possesses a $U(3)$ flavor symmetry under which ψ_i, ϕ_i transform as fundamentals. The model is thus consistent with minimal flavor violation and forbids new sources of flavor-changing neutral currents (FCNC). Note that the $U(3)$ flavor symmetry is optional for the purpose of suppressing FCNC: with couplings $10^{-7} \lesssim \alpha \lesssim 0.1$, there is no effect on the prediction for matter abundances in our model, while the FCNC constraint can be satisfied. Nevertheless with $\alpha \lesssim 0.1$ the potential DM direct detection signal (Sec. 2.4.2) would be too small to be observed. CP-violating Y_1 decays produce asymmetries in intermediate states ϕ and ψ and their conjugates. These states subsequently decay to produce asymmetries between udd and χ and their conjugates. For simplicity, we have taken the different flavors of ψ and ϕ to be degenerate in mass.

This will be the case throughout the rest of this chapter. The Feynman diagram for the decay chain is shown in Fig. 2.2. The above symmetries allow additional interactions between the Majorana singlet and the SM through $\bar{L}HY_1$ which permit decays $Y_1 \to Hl$. It is technically natural for this coupling to remain small such that Y_1 decays to $\phi\psi$ are dominant. Alternatively, the Yukawa interaction $\bar{L}HY_1$ is forbidden by imposing an exact Z_4 symmetry with the following charge assignments: Y_1 charge -1, $\psi,\ \phi,\ \chi$ charge i, and all SM charges are $+1$. This Z_4 symmetry also ensures the stability of asymmetric dark matter candidate χ.

Just like with WIMP DM freezeout, there are various possibilities of Y_1 annihilations that can lead to a metastable WIMP abundance through thermal freezeout. Our core mechanism and result (e.g. Eq. 2.2) are insensitive to the detailed realization of such annihilations/freezeout. To give a concrete example, we consider the simple case where Y_1, χ annihilate into SM singlet scalar S. Feynman diagrams for Y_1 and χ annihilation are shown in 2.3 and 2.4, respectively. This is the simplest case: there are more complex possibilities to realize Y_1 freezeout, e.g., broken $U(1)'$ gauge mediated Y_1 annihilation to $\psi,\ \phi,\ \chi$ [81,82].

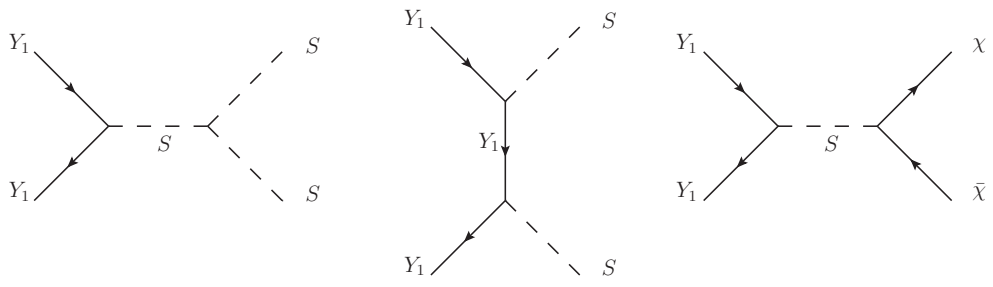

Figure 2.3: Annihilation processes that potentially contribute to Y_1 freezeout.

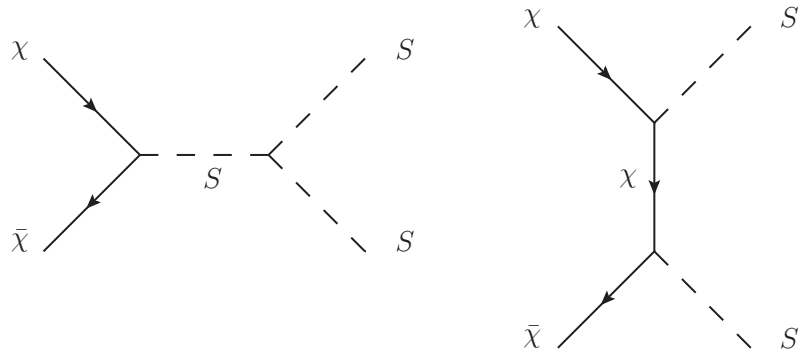

Figure 2.4: Annihilation process that depletes the symmetric component of $\chi\bar{\chi}$.

Specifically, for Y_1 freeze-out and χ symmetric component depletion, we introduce additional interactions as follows:

$$\mathcal{L}_{\text{f.o.}} \quad = \quad -\rho_{1,2} S \bar{Y}_{1,2} Y_{1,2} - \delta S \bar{\chi}\chi - \mu S^3 \tag{2.4}$$

There may be additional interactions for S such as $S\bar{\psi}\psi$ and $|\phi|^2 S^2$. These would permit further contributions to the Y_1 annihilation cross section. That said, the interactions in Eq. 2.4 constitute a minimal, renormalizable model for Y_1 freeze-out and ADM symmetric component depletion.

In order to efficiently deplete the symmetric component of χ, its annihilation cross section must be $\sigma_0(\chi\bar{\chi} \to SS) \gtrsim$ few $\times\, \sigma_{0,\text{WIMP}}$ [83]. The cross sections, σ_0 are defined by $\langle\sigma|\vec{v}|\rangle = \sigma_0(T/m)^n$ ($n = 0$ for s-wave annihilation, $n = 1$ for p-wave) and $\sigma_{0,\text{WIMP}} \approx 5 \times 10^{-26}$ cm^3/s. Following Eq. 2.4, ADM candidate χ undergoes t- and s-channel annihilations to S. In the $m_\chi \gg m_S$ limit, the cross section is $\sigma_0(\chi\bar{\chi} \to SS) = 3\delta^2\left[24\delta^2 - (20\mu\delta/3m_\chi) + (\mu^2/2m_\chi^2)\right]/64\pi m_\chi^2$. To give an example, for $\delta = 0.2$, $\mu = 5$ GeV and $m_\chi = 2.5$ GeV, the cross section is $\sigma_0(\chi\bar{\chi} \to SS) \approx 3\times10^{-22}$ cm$^3/s$ which is sufficiently

efficient to deplete the symmetric component of χ. Without a symmetry protection, S may decay to the SM states, e.g. through a mixing with the SM Higgs enabled by an $S|H|^2$ term. Thus the χ asymmetry remains the dominant contribution to the DM abundance.

With these interactions we can also define a generalized global baryon symmetry $U(1)_{B+2X}$ with conserved number G. We will further explain the G charge assignments in Sec. 2.2.4. The generalized baryon and other charges are given in Table 2.1.

	$SU(3)_C$	$SU(2)_L$	$U(1)_Y$	$U(1)_{B+2X}$	Z_4
$Y_{1,2}$	**1**	**1**	0	0	-1
ψ	$\bar{\mathbf{3}}$	**1**	$+2/3$	$+1/6$	$+i$
ϕ	**3**	**1**	$-2/3$	$-1/6$	$+i$
χ	**1**	**1**	0	$-1/2$	$+i$
S	**1**	**1**	0	0	$+1$
u	**3**	**1**	$+4/3$	$+1/3$	$+1$
d	**3**	**1**	$-2/3$	$+1/3$	$+1$

Table 2.1: Quantum numbers of the relevant particles in WIMP cogenesis with baryons.

After the decay processes have taken place, efficient matter-antimatter annihilations deplete the $\bar{\chi}$ number density to near triviality. This leaves an abundance of two χ's for every unit of baryon number (udd). The shared interactions fix the relationship between the asymmetries of baryons and χ. This then fixes the ADM χ mass according to Eq. 2.1. It is apparent that $n_{B-L}/n_{DM} = 1/2$ for this model. $c_s \equiv \frac{n_B}{n_{B-L}}$ characterizes the potential effect of redistribution among B and L numbers due to sphaleron interactions. If the asymmetry is produced after the electroweak phase transition (EWPT), $c_s = 1$. If the asymmetry is produced before EWPT [84], SM charged particles and ϕ, ψ, χ are in chemical equilibrium and their chemical potentials are related by the active gauge and Yukawa interactions as well as sphaleron processes. With the SM alone, $B - L$ is preserved, while

in this model the linear combination $B - L + 2X$ is conserved. Putting all these together we can solve for c_s. As explained in Appendix A, c_s has a dependence on the masses of ψ, ϕ relative to the temperature at EWPT, $T_{\rm EWPT}$. Given the large uncertainty in determining $T_{\rm EWPT}$, we consider two limits of interest which would define the range of the c_s values: $m_{\phi,\psi} \ll T_{\rm EWPT}$ and $m_{\phi,\psi} \gg T_{\rm EWPT}$. The solutions for the two limits are (details given in Appendix A.1):

$$c_s = \frac{n_B}{n_{B-L}} = \begin{cases} \frac{4(N_f+N_H)}{14N_f+13N_H} & m_{\phi,\psi} \ll T_{\rm EWPT} \\ \frac{8N_f+4N_H}{22N_f+13N_H} & m_{\phi,\psi} \gg T_{\rm EWPT} \end{cases} \tag{2.5}$$

where N_f and N_H are the number of generations of fermions and number of Higgs, respectively. For matter asymmetries produced before EWPT with $N_f = 3$ and $N_H = 1$ Eq. 2.5 gives $c_s = 16/55$ for $m_{\phi,\psi} \ll T_{\rm EWPT}$ or $c_s = 28/79$ for $m_{\phi,\psi} \gg T_{\rm EWPT}$. Combining these and Eq. 2.1, we find that $m_\chi = 2.5$ GeV if the asymmetry is produced after EWPT and $m_\chi \approx 0.72$ GeV $- 0.89$ GeV if produced before EWPT.

Next we demonstrate how WIMP cogenesis satisfies the Sakharov conditions [18] for generating a primordial asymmetry in both baryon and DM sectors.

2.2.2 WIMP Freezeout and the Generalized WIMP Miracle

The thermal freezeout of Y_1 provides the out-of-equilibrium condition for asymmetry generation upon the subsequent decays.

The freezeout of Y_1 proceeds through S mediated annihilation to the hidden sector states S, χ. The annihilation rate is given by $\Gamma(Y_1 Y_1 \to \chi\bar{\chi}, SS) = n_Y \langle \sigma(Y_1 Y_1 \to \chi\bar{\chi}, SS)|\vec{v}|\rangle$. Since Y_1 and χ couple to scalar S, there is no s-wave contribution to the

cross section because of helicity suppression in the fermionic case and the imposition of CP-invariance in the scalar case [85]. Although pseudoscalar coupling to S would lift this suppression, velocity suppressed annihilation is sufficient, as we will see in Sec. 2.2.6. The p-wave contributions to the Y_1 annihilation cross section are to $\chi,\ S$ final states, as shown in Fig. 2.3. The freezeout occurs at $T_{f.o.}$ when the Y_1 annihilation rate falls below the Hubble expansion rate, which can be estimated as follows:

$$x_{f.o} \equiv \frac{m_1}{T_{f.o.}} \simeq \ln\left\{\frac{0.152 g_*^{-1/2} M_{\rm Pl} m_1 \sigma_0}{\ln^{3/2}\left(0.152 g_*^{-1/2} M_{\rm Pl} m_1 \sigma_0\right)}\right\} \tag{2.6}$$

where we parametrize the p-wave contributions to the thermally averaged cross-section in the limit $m_1 \gg m_S$ as $\langle \sigma_{Y_1 \rm ann} |\vec{v}| \rangle \simeq \sigma_0 x^{-1}$ with

$$\sigma_0 = \frac{3(24\rho_1^4 - \frac{20\rho_1^3\mu}{3m_1} + \frac{\mu^2\rho_1^2}{2m_1^2} + \delta^4)}{64\pi m_1^2} \tag{2.7}$$

where $M_{\rm Pl} = 1.2\times10^{19}$ GeV is the Planck mass and g_* is the effective degrees of freedom [86]. Since efficient depletion of the symmetric component of ADM requires $m_S \lesssim m_\chi \sim \mathcal{O}(\text{GeV})$ while $m_1 \sim \mathcal{O}(\text{TeV})$, we take $m_1 \gg m_S \to 0$ and σ_0 in the non-resonant region. For example, with $m_1 \approx 5$ TeV WIMP with freeze-out Yukawa couplings $\delta \approx 0.2$, $\rho_1 = 0.08$, and $\mu = 5$ GeV, Y_1 freezes out as a cold relic with $T_{\rm f.o.} \approx \frac{m_1}{16.5} \approx 303$ GeV. Its comoving density $Y_{Y_1} \equiv \frac{n_{Y_1}}{s}$ at the time of freezeout is given by [16]

$$Y_{Y_1,\rm f.o.} = \frac{7.58 g_*^{1/2} x_{f.o.}^2}{g_{*S} M_{\rm Pl} m_1 \sigma_0}, \tag{2.8}$$

where g_{*S} is the effective number of degrees of freedom in entropy. Note that if Y_1 does not decay, its would-be relic abundance today $Y_{Y_1}^{\tau\to\infty} \approx Y_{Y_{1,\rm f.o.}}$

Following the schematic illustration in Fig. 2.1, we expect the observed abundances of DM and baryons to be proportional to the freeze out abundance found in Eq. 2.8.

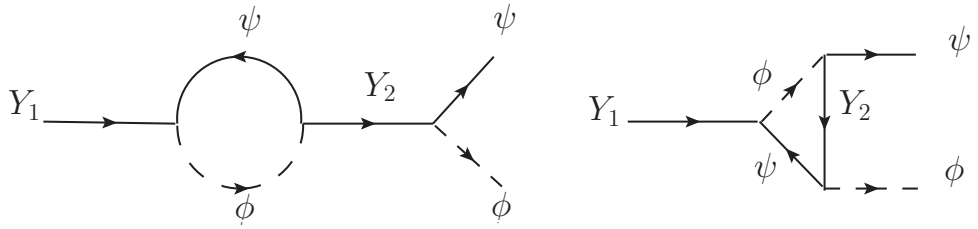

Figure 2.5: Loop diagrams interfere with the tree-level diagram to produce a nonzero asymmetry between Y_1 decays to ϕ/ψ and $\phi^*/\bar{\psi}$

2.2.3 C and CP Violation

C- and CP-violation are achieved by the decay of the Majorana fermions Y_1 following their freeze out. The CP asymmetry arising from Y_1 decays is defined as

$$\epsilon_1 = \frac{\Gamma(Y_1 \to \phi\bar{\psi}) - \Gamma(Y_1 \to \phi^*\psi)}{\Gamma(Y_1 \to \phi\bar{\psi}) + \Gamma(Y_1 \to \phi^*\psi)} \tag{2.9}$$

The denominator of Eq. 2.9 can be approximated as twice the tree-level decay rate, $\Gamma_0(Y_1 \to \phi\bar{\psi})$. For complex WIMP Yukawa couplings, interference between the tree-level and loop-level Feynman diagrams shown in Fig. 2.5 gives rise to a non-vanishing numerator in Eq. 2.9. Although in analogy Y_2 decay may generate a CP asymmetry as well, its contribution to the DM/baryon asymmetry is generally washed out with $m_2 > m_1$ and $|\eta_1| \ll |\eta_2|$ (leading to sizable ϵ_1 but in-equilibrium decay of Y_2).

In many baryogenesis models based on massive particle decay, the decay products are much lighter than the decaying particle and thus can be approximately taken as massless. For WIMP cogenesis we include full mass-dependence since WIMP freezeout generically requires $m_1 \sim \mathcal{O}(100)$ GeV $-$ 10 TeV while the intermediate decay products ϕ and ψ are experimentally constrained to have masses $\gtrsim O(100)$ GeV $- O$(TeV) (Sec. 2.4.1).

With this in mind and using the Optical Theorem, we find the CP-asymmetry:

$$\epsilon_1 \;=\; -3\frac{\sqrt{xa}\mathrm{Im}\big[(\eta_2^*\eta_1)^2\big]}{8\pi|\eta_1|^2 b^2}\left\{\frac{1}{1-x}+b^2+c^2\ln\left[\frac{c^2+\frac{b^2}{2a}(1-a)}{c^2+\frac{b^2}{2a}(1+a)}\right]\right\} \tag{2.10}$$

where $a \equiv (1+\frac{m_\psi^2-m_\phi^2}{m_1^2})^{-2}\big[(1-\frac{m_\psi+m_\phi^2}{m_1^2})^2-\frac{4m_\psi^2 m_\phi^2}{m_1^4}\big]$, $b^2 \equiv a\big(1+\frac{m_\psi^2-m_\phi^2}{m_1^2}\big)^2$, $c^2 \equiv \frac{2m_\phi^2-m_1^2-m_2^2}{m_1^2}$ and $x=\frac{m_2^2}{m_1^2}$. The factor of 3 represents the color multiplicity. Note this is the contribution to the CP-asymmetry of Y_1 decays to a single generation. To simplify our analyses, we assume the three flavors of ϕ and ψ are (nearly) degenerate in mass. Under this assumption, there is an additional multiplicative factor of 3 to account for the contributions Y_1 decays to the all flavors. Also note that Eq. 2.10 reproduces the familiar CP-asymmetry result for leptogenesis [87] in the limit of $m_1 \gg m_{\psi,\phi}$. The above expression shows how the asymmetry is intimately tied to the mass and couplings of the $Y_1,\ m_\phi,$ and m_ψ. In Section 2.2.6, we show contours of constant Ω_{DM} in the (m_1,ρ) plane with ϵ_1 taking the form of Eq. 2.10.

2.2.4 Generalized Baryon Number Conservation and Generation of Asymmetries

In order for a matter asymmetry to be produced, the corresponding baryon or DM number must be violated by the interactions in the model. In this model both SM baryon number and DM number are violated in the last stage of the decay chain as illustrated in Fig. 2.2. Nevertheless a generalized baryon number $G = B + 2X$ is conserved (remains 0 with no pre-existing asymmetry) thanks to shared interactions between $\chi,\ \psi,\ \phi$ and quarks.

The CP-violation in Y_1 decay (Section 2.2.3) produce an asymmetry between intermediate states (i.e., baryon/ADM parents), ϕ and ψ and their conjugates, which is inherited by their decay products, χ and udd, and ultimately becomes the source of all (asymmetric)

matter today. The changes in the generalized baryon number for each decay process are given by:

$$\Delta G_{Y_1 \to \phi\psi} = G_\phi + G_\psi - G_{Y_1} \tag{2.11}$$

$$\Delta G_{\phi \to \chi d} = 1/3 + G_\chi - G_\phi \tag{2.12}$$

$$\Delta G_{\psi \to \phi u} = 1/3 + G_\phi - G_\psi, \tag{2.13}$$

where we have used the fact that for quarks $G_q = B_q = 1/3$. Furthermore, due to the Majorana nature of Y_1, its natural $U(1)_{B+2X}$ charge is $G_{Y_1} = 0$. Then requiring all the above interactions to conserve G, we may obtain the solutions for the charge assignments: $G_\chi = -1/2$, $G_\phi = -G_\psi = -1/6$, as listed in Table. 2.1. The net result of the decay chain is $udd + \chi\chi$, violating the SM baryon number and DM number by 1 and 2 units respectively, while the net generalized baryon number G is conserved. So the generalized baryonic charge carried by the ADM density cancels that of a baryon asymmetry density and the universe has trivial net generalized baryon number.

2.2.5 WIMP Decays and Production of Matter Asymmetries

We consider the asymmetry grandparent, Y_1, decays well after its freezeout but before BBN, i.e., $1\text{MeV} \lesssim T_{Y_1,\text{dec}} \lesssim T_{\text{f.o.}}$, so that we can treat the freezeout and decay-triggered cogenesis as nearly decoupled processes and retain the conventional success of BBN. The Y_1 decay rate at $T < m_1$ is $\Gamma_{Y_1,\text{dec}} \approx \frac{|\eta_1|^2 m_1}{8\pi}$. Following Eq. 2.6, the freezeout occurs around the temperature $T_{\text{f.o.}} \sim 200 - 300$ GeV for TeV-scale mass Y_1. The requirement that it decay between freezeout and BBN gives the range of allowed decay couplings: $10^{-15} \lesssim |\eta_1| \lesssim 10^{-9}$. For simplicity we assume the subsequent SM B- and DM χ-number

violating decay of ϕ, ψ to udd, χ are prompt relative to H, i.e., in equilibrium, so that the matter asymmetries are immediately distributed upon Y_1 decay. This assumption also simplifies the Boltzmann equations, since n_ψ, n_ϕ can be set as equilibrium distribution.

With Y_1 freezeout occurring well before its decay, the late-time evolution of co-moving density Y_{Y_1} satisfies the following Boltzmann equation for a decaying species:

$$\frac{dY_{Y_1}}{dx} = \frac{-x\langle\Gamma(Y_1 \to \phi\psi)\rangle}{2H(m_1)}(Y_{Y_1} - Y_{Y_1}^{\rm eq})$$

where $x = m_1/T$ and $H(m_1) = H(T = m_1)$. The initial condition for Y_{Y_1} of this stage of evolution is set by the would-be abundance of Y_1 after its freezeout: $Y_{Y_1}(0) \approx Y_{Y_1,\rm f.o.}$ where $Y_{Y_1,\rm f.o.}$ is given in Eq. 2.8.

We now write down the Boltzmann equations governing the evolution of ϕ, ψ number densities. This evolution is determined by three processes: CP-violating Y_1 decays and their inverse, Y_1 mediated ϕ/ψ scattering to their conjugates (and vice versa), and CP-conserving ϕ/ψ (as well as their conjugates) decays.

For convenient notations, we define the generalized baryon number density n_G which is the sum of ϕ/ψ asymmetries:

$$n_G = \frac{n_\phi - n_{\phi^*}}{2} + \frac{n_\psi - n_{\bar\psi}}{2} \tag{2.14}$$

Once simplified, the ϕ asymmetry, $n_\phi - n_{\phi^*} \equiv n_{\Delta\phi}$ evolves according to

$$\begin{aligned}
\dot n_{\Delta\phi} + 3Hn_{\Delta\phi} &= \epsilon_1\langle\Gamma(Y_1 \to \phi\psi)\rangle(n_{Y_1} - n_{Y_1}^{\rm eq} - \frac{Y_G}{2\epsilon_1}n_{Y_1}^{\rm eq}) - 2n_G n_\gamma\langle\sigma(\phi\psi \to \phi^*\bar\psi)|\vec v|\rangle \\
&- \langle\Gamma(\phi \to \chi + d)\rangle\big[(n_\phi - n_\phi^{\rm eq}) - (n_{\phi^*} - n_{\phi^*}^{\rm eq})\big] \\
&+ \langle\Gamma(\psi \to \phi + u)\rangle\big[(n_\psi - n_\psi^{\rm eq}) - (n_{\bar\psi} - n_{\bar\psi}^{\rm eq})\big],
\end{aligned} \tag{2.15}$$

where ϵ_1 is the CP asymmetry given in Eq. 2.10, $\langle\Gamma\rangle$'s are thermally averaged decay rates, $Y_G \equiv \ n_G/s = \frac{1}{2s}[(n_\phi - n_{\phi^*}) + (n_\psi - n_{\bar{\psi}})]$, and n_γ is the photon radiation density. The equation governing the cosmological evolution of the ψ asymmetry is

$$\begin{aligned} \dot{n}_{\Delta\psi} + 3Hn_{\Delta\psi} &= \epsilon_1\langle\Gamma(Y_1 \to \phi\psi)\rangle(n_{Y_1} - n_{Y_1}^{\rm eq} - \frac{Y_G}{2\epsilon_1}n_{Y_1}^{\rm eq}) - 2n_G n_\gamma\langle\sigma(\phi\psi \to \phi^*\bar{\psi})|\vec{v}|\rangle \\ &- \langle\Gamma(\psi \to \phi + u)\rangle\big[(n_\psi - n_\psi^{\rm eq}) - (n_{\bar{\psi}} - n_{\bar{\psi}}^{\rm eq})\big] \end{aligned} \tag{2.16}$$

We can see that the main difference between the ϕ and ψ Boltzmann evolution is that the term governing ψ decays changes sign and there is no term for ψ-number increasing ϕ decays. Note that in these evolution eqs., the terms proportional to Y_G can potentially wash out the produced asymmetries (inverse decay of Y_1 and the 2-2 scattering). Assuming prompt ϕ, ψ decays, we set $n_\phi = n_\phi^{\rm eq}, n_\psi = n_\psi^{\rm eq}$, such that the contribution from these decays vanish. Additional potential washout processes of $udd\chi\chi \to Y_1$ and $udd\chi\chi \to \bar{u}\bar{u}\bar{d}\bar{\chi}\bar{\chi}$ are negligible owing not only to Boltzmann suppression, but also to the high dimension of the effective operators responsible for these processes.

Based on Fig. 2.2 and our earlier discussion, upon decays of ϕ and ψ, n_G or Y_G leads to baryon asymmetry density n_B and DM asymmetry density n_χ with the robust relation:

$$n_G = (n_{\Delta\phi} + n_{\Delta\psi})/2 = n_B = n_\chi/2 \tag{2.17}$$

The general solution of the Boltzmann equations gives the comoving generalized matter asymmetry Y_G today:

$$\begin{aligned} Y_G(0) &= \epsilon_1 \int_0^{T_{dec}} \frac{dY_{Y_1}}{dT} \exp\Big(-\int_0^T \frac{\Gamma_W(T')}{H(T')}\frac{dT'}{T'}\Big)dT \\ &+ Y_B^{\rm initial} \exp\Big(-\int_0^{T_{\rm initial}} \frac{\Gamma_W(T)}{H(T)}\frac{dT}{T}\Big) \end{aligned} \tag{2.18}$$

where Γ_W is the rate of processes washing out the asymmetry. Assuming that there is no primordial asymmetry before WIMP cogenesis occurs, $Y_B^{\text{initial}} = 0$. Taking our simplifying assumption that Y_1 decays well after its freeze out, we automatically work in the weak washout regime and drop the exponential factor in Eq. 2.18. This yields a robust solution depending solely on the would-be WIMP miracle abundance of Y_1 and the CP asymmetry ϵ_1:

$$Y_B(\infty) = Y_\chi(\infty)/2 = Y_G(\infty) \approx \epsilon_1 Y_{Y_1,\text{f.o.}} \tag{2.19}$$

Provided efficient annihilation that depletes the symmetric component of χ, the above asymptotic solution of n_B, n_χ give rise to the baryon and DM abundances today:

$$\Omega_\chi(\infty) = \frac{2m_\chi s_0}{\rho_c}\epsilon_1 Y_{Y_1,\text{f.o.}} \tag{2.20}$$

$$\Omega_B(\infty) = \frac{c_s m_n s_0}{\rho_c}\epsilon_1 Y_{Y_1,\text{f.o.}}, \tag{2.21}$$

where $s_0 = 2970$ cm^{-3} is the radiation entropy density today and $\rho_c = 3H_0^2/8\pi G \approx 3.5 \times 10^{-47}$ GeV^4 is the critical energy density, $m_n \approx 1$ GeV is the SM baryon mass. ϵ_1, $Y_{Y_1,\text{f.o.}}$ have been calculated in earlier sections. Based on the discussion about c_s and Eq. 2.1 in Sec. 2.1 , the observed relation $\Omega_{DM} \approx 5\ \Omega_B$ fixes $m_\chi = 2.5$ GeV or $m_\chi = 0.72 - 0.89$ GeV for Y_1 decay after or before EWPT, respectively.

2.2.6 Numerical Results

We now scan parameter space to demonstrate viable regions that predicts $\Omega_\chi = \Omega_{\rm DM} \approx 5\Omega_B$ as observed. The relevant parameters includes the masses ($m_1,\ m_2,\ m_\phi,\ m_\psi,\ m_\chi,\ m_S$) and couplings ($\eta_1,\ \eta_2,\ \rho,\ \delta,\ \mu$). We take η_1 to be real such that the CP-asymmetry in Eq. 2.10 can be written in terms of a complex phase of η_2: $\mathrm{Im}[(\eta_1^*\eta_2)^2] \to |\eta_1|^2|\eta_2|^2 \sin(2\theta_2)$. In our analyses, we fix $\theta_2 = \pi/4$ to bound the CP-asymmetry from above.

Due to the color charges of ϕ and ψ, their masses are effectively constrained by collider experiments (see Section 2.4.1). This immediately constrains the mass of the lighter of the Majorana fermion $m_1 \gtrsim 3$ TeV such that $Y_1 \to \phi\psi$ remains kinematically open for $m_\psi \gtrsim m_\phi \sim$ TeV. The symmetric component of ADM is efficiently depleted through annihilations to the hidden sector, e.g. $\chi\bar{\chi} \to SS$, which requires $m_\chi > m_S$ such that the annihilation process is kinematically open.

Taking benchmark values of $m_2 \gtrsim 10$ TeV, $m_\phi \approx 1.2$ TeV, $m_\psi \approx 1.7$ TeV, $\delta = 0.2$, and $\mu \approx 5$ GeV, with *Mathematica* [88] we plot contours of $\Omega_{DM}h^2 = 0.120 \pm 0.001$, $\Omega_B h^2 = 0.0224 \pm 0.0001$ [15] in the (m_1, ρ_1) plane, as shown in Fig. 2.6. Because the baryon asymmetry is directly produced by Y_1 decays, it may be produced before or after the EWPT. Comparing the case of Y_1 decay before vs. after EWPT, we see that a smaller Y_1 Yukawa coupling to S and larger m_1 (for a given $|\eta_2|$) are required to produce the observed DM abundance when the asymmetry is produced before EWPT due to the sphaleron's moderate washout of the SM baryon asymmetry. This is because $Y_{Y_1,\text{f.o.}} \sim 1/\sigma_0 \sim m_1^2/\rho_1^4$ giving a larger decaying Y_1 abundance to compensate for this washout. The CP-asymmetry produced by Y_1 decays, as given in Eq. 2.10, must be sufficient to produce the observed

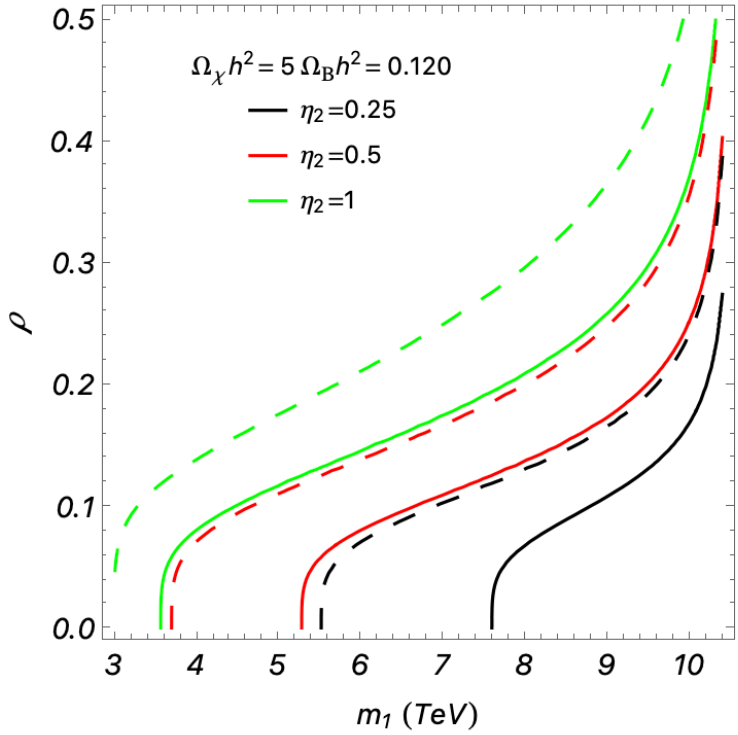

Figure 2.6: Contours of Ω_χ, Ω_B as a function of Yukawa coupling ρ_1 and Y_1 mass m_1 for different values of η_2 in WIMP cogenesis for baryons. The solid (dashed) lines correspond to the case where asymmetries in DM and baryons are produced before (after) the EWPT with $m_\chi = 0.72$ GeV ($m_\chi = 2.5$ GeV). The benchmark parameters used are: $\delta = 0.2$, $\mu = 5$ GeV, $m_S \to 0$ GeV, $m_\phi = 1.2$ TeV, $m_\psi = 1.7$ TeV, and $m_2 = 10.5$ TeV.

abundances of DM and baryons for $\rho \sim 0.1$ (as discussed in Sec. 2.2.1) and $m_1 \sim \mathcal{O}$ (TeV). To give an example, with Y_1 Yukawa coupling $\eta_2 = 0.5$, $m_2 = 10.5$ TeV, $m_1 = 5$ TeV, $m_\psi = 1.7$ TeV, and $m_\phi = 1.2$ TeV the CP-asymmetry is $|\epsilon_1| \approx 1\%$.

2.3 WIMP Decay to Leptons and ADM

In the following section, we present a WIMP cogenesis model that directly produces a lepton asymmetry. As with other models of leptogenesis, the asymmetry must be produced before EWPT such that sphalerons may transfer the lepton asymmetry into the observed

baryon asymmetry. Here, we introduce the fields, interactions, and discuss the differences from WIMP cogenesis with baryons presented in the last section.

2.3.1 Model Setup

The first two stages of WIMP cogenesis with leptons are identical to the model discussed above: the Majorana fermion, Y_1, undergoes freezeout via Yukawa and cubic interactions with singlet scalar S followed by out-of-equilibrium and CP-violating decays to (unstable) intermediate states ϕ and ψ. Again, the Majorana fermion, Y_1, is a SM gauge singlet, but now the intermediate states are charged under SM $SU(2)_L \times U(1)_Y$, such that the decays $\psi^0 \to \chi h,\ \chi Z$, $\psi^\pm \to \chi W^\pm$ and $\phi \to \chi \ell$ are possible, where $h, W^\pm, Z, \ell$ are the SM Higgs, electroweak gauge bosons, and left-handed leptons, respectively. The Lagrangian is identical to that in Eqs. 2.3 and 2.4 up to modification of the Yukawa interactions:

$$\mathcal{L}_{\text{Yukawa}} \to -\alpha_{ijk}\phi_i \bar{L}_i \chi_k^c - \beta_{ii} H \bar{\psi}_i \chi_i \tag{2.22}$$

where L is the left-handed lepton doublet, H is the Higgs doublet, $i = 1, 2, 3$ is flavor indices, and α_{ijk} is antisymmetric in flavor indices. Note that this model possesses a $U(3)$ flavor symmetry which prevents new sources of FCNC. As discussed in Sec. 2.2 the U(3) symmetry is optional provided that $10^{-7} \lesssim \alpha \lesssim 0.1$, while the DM direct detection signal may be absent with such small couplings. The charge assignments are summarized in Table 2.2. A Z_4 symmetry is imposed to ensure DM stability and prevent Y_1 decay through $Y_1 LH$ portal. The decay chain is illustrated in Fig.2.7. The CP asymmetry is generated by the same process as illustrated in Fig. 2.5.

	$SU(3)_C$	$SU(2)_L$	$U(1)_Y$	$U(1)_{L+2X}$	Z_4
$Y_{1,2}$	$\mathbf{1}$	$\mathbf{1}$	0	0	-1
ψ	$\mathbf{1}$	$\bar{\mathbf{2}}$	$+1$	$-1/2$	$+i$
ϕ	$\mathbf{1}$	$\mathbf{2}$	-1	$+1/2$	$+i$
χ	$\mathbf{1}$	$\mathbf{1}$	0	$-1/2$	$+i$
S	$\mathbf{1}$	$\mathbf{1}$	0	0	$+1$
L	$\mathbf{1}$	$\mathbf{2}$	-1	$+1$	$+1$
H	$\mathbf{1}$	$\bar{\mathbf{2}}$	$+1$	0	$+1$

Table 2.2: Quantum numbers of the relevant particles in WIMP cogenesis with leptons.

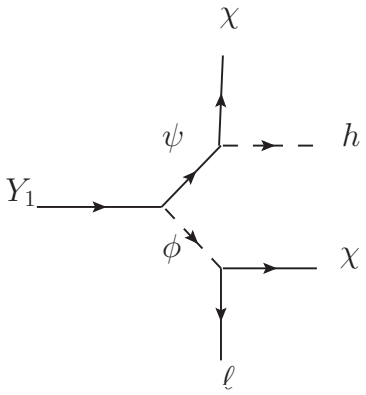

Figure 2.7: Feynmann diagram of the decay chain for WIMP cogenesis with leptons. ψ may also decay to electroweak gauge bosons Z and $W^{\pm}$

In analogy to WIMP cogenesis with baryons, the shared interactions through intermediate ϕ, ψ permit a generalized global lepton number symmetry $U(1)_{L+2X}$ with conserved charge G'. The corresponding charge assignment is: $G'_{\chi} = 1/2$, $G'_{Y_1} = 0$, $G'_{\phi} = 1/2$, and $G'_{\psi} = -1/2$. As shown in Fig. 2.7, the second stage of the decay chain violates SM lepton and DM number, giving rise to 1 unit of L-number and 2 units of X-number. After all the decays have taken place, efficient annihilations deplete the symmetric components of ADM and leptons, leaving an abundance of χ and L. A key difference from the model in Sec. 2.2 is that the asymmetry must be produced before EWPT such that sphalerons convert the lepton asymmetry into the observed baryon asymmetry, i.e., $T_{\rm f.o} > T_{\rm dec} \gtrsim T_{\rm EWPT}$. As in

the quark model, $\chi\bar{\chi}$ depletion occurs through annihilation to S. This depletion may also receive contributions from ϕ-mediated annihilation to leptons, due to the weaker constraints on ADM-lepton couplings (relative to ADM-quark couplings) [89]. Feynman diagrams for these processes are shown in Fig. 2.8.

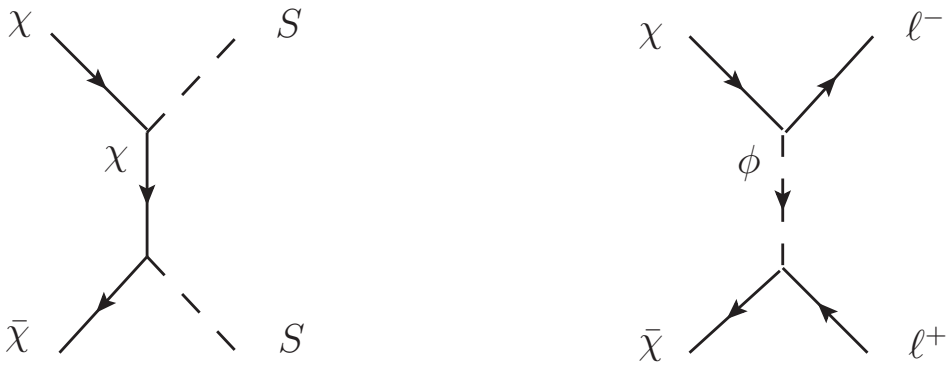

Figure 2.8: Diagrams contributing to $\chi\bar{\chi}$ depletion.

We can then apply most results from Sections 2.2.2-2.2.5 by analogy, with some modifications. The most straightforward change is the dropping of the color factor in the CP-asymmetry of Eq. 2.10. More subtle is the change to the DM mass prediction. Due to the different Yukawa interactions, the prediction of the relation $c_s = \frac{n_B}{n_{B-L}}$ in this model differs from that in the WIMP cogenesis with baryons. In addition, as noted, WIMP cogenesis with leptons needs to occur before EWPT when sphaleron processes are active. The limits of interest are the same as those detailed in the previous section. The solutions

in these two limits are (see Appendix A.2)

$$c_s = \frac{n_B}{n_{B-L}} = \begin{cases} \frac{8N_f+4N_H}{30N_f+13N_H} & m_{\phi,\psi} \ll T_{\rm EWPT} \\ \frac{8N_f+4N_H}{22N_f+4N_H} & m_{\phi,\psi} \gg T_{\rm EWPT} \end{cases} \tag{2.23}$$

where N_F and N_H are again the number of generations of fermions and Higgs, respectively. With $N_f \to 3$ and $N_H \to 1$ in Eq. 2.23 with gives $c_s = 28/103$ for $m_{\phi,\psi} \ll T_{\rm EWPT}$ or $c_s = 28/79$ for $m_{\phi,\psi} \gg T_{\rm EWPT}$. All together, the relation between lepton, baryon, and ADM comoving densities is akin to Eq. 2.19: $Y_L = Y_\chi/2 = \frac{|c_s-1|}{c_s} Y_B$. Following the same procedure as Sec. 2.2.5, in the weak washout regime we obtain ADM abundance with the same form as Eq. 2.20:

$$\Omega_\chi(\infty) = \frac{2m_\chi s_0}{\rho_c} \epsilon_1 Y_{Y_1,\text{f.o.}} \tag{2.24}$$

$$\Omega_B(\infty) = \frac{c_s m_n s_0}{|c_s-1|\rho_c} \epsilon_1 Y_{Y_1,\text{f.o.}}. \tag{2.25}$$

The observed ratio $\Omega_{DM}/\Omega_B \approx 5$ fixes the mass of the ADM candidate $m_\chi = \frac{5c_s}{2|c_s-1|} m_n$. With the values for c_s given in Eq. 2.23, the range of χ masses is $0.93-1.37$ GeV.

2.3.2 Numerical Results

We now scan model parameters to find viable region giving the observed matter abundances. The relevant parameters includes the masses ($m_1,\ m_2,\ m_\phi,\ m_\psi,\ m_\chi,\ m_S$) and couplings ($\eta_1,\ \eta_2,\ \rho,\ \delta,\ \mu$). We also take the same parametrization for the CP-asymmetry relevant Yukawa couplings, η_1 and η_2, as in Sec. 2.2.6.

The constraints arising from colliders on exotic electroweak states (ϕ and ψ in this model) are less stringent than those on exotic colored states, allowing us to explore sub-TeV masses for ϕ, ψ, and even the grandparent, Y_1. There is a caveat to this: if the mass of

the decaying WIMP is too light, it freezes out *after* the EWPT, thus its lepton asymmetry producing decays would occur when sphaleron processes, necessary for the conversion into the observed baryon asymmetry, are no longer effective. For Y_1 decays to happen after freezeout, but before EWPT, we require 100 GeV $\lesssim T_{Y,\mathrm{dec}} \lesssim T_{\mathrm{f.o}}$. With a $m_1 \sim 1$ TeV, the freezeout occurs at or just after EWPT, according to Eq. 2.6.

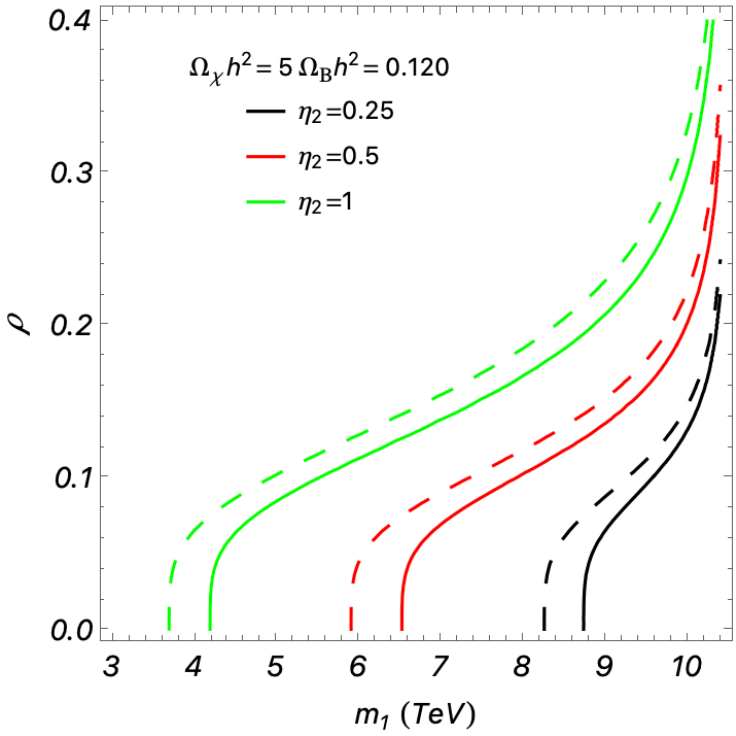

Figure 2.9: Contours of Ω_χ, Ω_B as a function of Yukawa coupling ρ_1 and Y_1 mass m_1 for different values of η_2 for WIMP cogenesis with leptons. The solid lines correspond to $m_\chi = 0.93$ GeV and dashed lines to $m_\chi = 1.37$ GeV, both cases with S mass $m_S = 0$ GeV. Other benchmark parameters are: $\delta = 0.2$, $\mu = 5$ GeV, $m_\phi = 700$ GeV, $m_\psi = 740$ GeV, and $m_2 = 10.5$ TeV.

Since ψ contributes to the matter asymmetry via $\psi^0 \to \chi h, \chi Z$, and/or $\psi^\pm \to \chi W^\pm$ it requires m_ψ greater than at least m_W. Similarly, since ϕ decays to $\mathcal{O}$(GeV) mass χ and SM leptons, $m_\phi \gtrsim \mathcal{O}$(GeV) is required. That said, collider constraints (see 2.4.1)

on new electroweak states require these states be much heavier than the above kinematic requirements. Fig. 2.9 shows the DM abundance as a function of Y_1-S Yukawa coupling and m_1, in the range of 1 TeV $< m_1 <$ 10 TeV. In these numerical analyses, we take the functional form of Eq. 2.10 and Eq. 2.8 for the CP-asymmetry and freezeout abundance of Y_1, respectively.

As can be seen in Fig. 2.9, a smaller coupling ρ_1 is required in the case with smaller m_χ. This is related to whether interactions of ψ, ϕ Yukawa and gauge interactions contribute to chemical equilibration along with sphalerons. When they contribute ($m_{\phi,\psi} \ll T_{\rm EWPT}$), there is further washout of the produced asymmetry. A smaller Yukawa coupling ρ compensates for this washout since $Y_\infty \propto \sigma^{-1}$.

2.4 Phenomenology and Constraints

2.4.1 Collider Phenomenology

WIMP Decay to Baryons and ADM (Sec. 2.2)

In the model where the WIMP decays to quarks (Sec. 2.2), SM charged colored scalars and fermions, ϕ_i and ψ_i respectively, are introduced. Owing to the color charges carried by these intermediate states, the LHC bounds on their masses are strong. As outlined in Sec. 2.2, ψ decays through intermediate scalar ϕ to 2 SM quarks and singlet ADM candidate χ, and ϕ decays to an SM quark and χ. These states are pair-produced at the LHC dominantly through gluon fusion, with subsequent decays $\phi \to j + \not{E}_T$, $\psi \to jj + \not{E}_T$, rendering typical signatures: $pp \to \psi\bar{\psi} \to 4j + \not{E}_T$ and $pp \to \phi\phi^* \to jj + \not{E}_T$. The

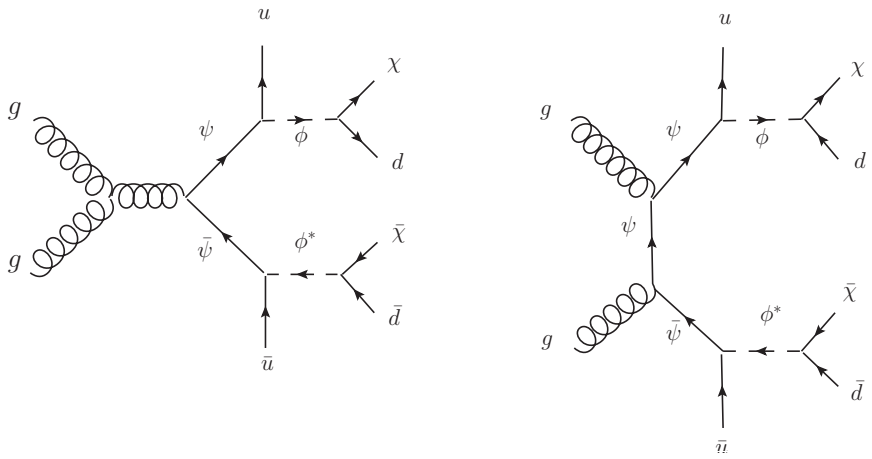

Figure 2.10: Diagrams relevant for ψ searches at hadron colliders (WIMP cogenesis with baryons).

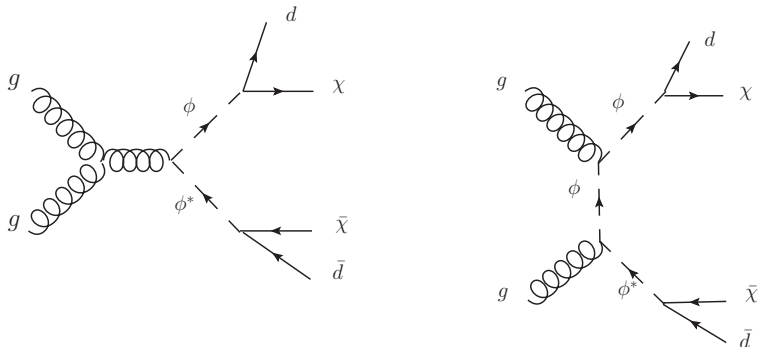

Figure 2.11: Diagrams relevant for ϕ searches at hadron colliders (WIMP cogenesis with baryons).

relevant diagrams are shown in Figs. 2.10 and 2.11.

LHC searches for squarks, $\tilde{q}$, and gluinos, $\tilde{g}$, in the presence of neutralino LSP $\tilde{\chi}_1^0$ are relevant for constraining the masses of ϕ and ψ in our model. In particular the bound in the massless LSP limit applies since the corresponding particle in WIMP cogenesis, χ has a mass of $\mathcal{O}(\text{GeV})$, significantly smaller than those of ϕ and ψ. Specifically, both ψ and $\tilde{g}$ decay to $jj + \not{E}_T$ via intermediate colored scalars with production cross sections differing only by a group theory factor, for which we correct. Simplified model searches at 13 TeV

from CMS with 137 fb^{-1} of data place bounds on the gluino mass in the presence of a massless LSP, neutralino $\tilde{\chi}_1^0$ [90]. The lower bound on the ψ mass is $m_\psi \gtrsim 1.3$ TeV which is from the gluino bound with the different group theory factor in cross section taken into account. In the case where the gluino decays to top quarks via intermediate top squark, the bound on the gluino mass is a bit stronger: $m_{\tilde{g}} \approx m_\psi \gtrsim 1.5$ TeV [90].

LHC searches for mass degenerate squarks bound the mass of ϕ, since both squarks and ϕ decay to $j + \not{E}_T$. The recent searches at CMS place bounds on three generations of mass degenerate squarks of $m_{\tilde{q}} \gtrsim 1.13$ TeV assuming massless LSP [90]. Since we make the assumption of three flavors of mass degenerate exotic scalar quarks ϕ_i in WIMP cogenesis, we apply this bound directly, leading to $m_\phi \gtrsim 1.13$ TeV.

Thus, for successful models where a matter asymmetry is produced from WIMP decays directly to baryons and ADM, the intermediate state masses are bound from below as $m_\psi \gtrsim m_\phi \sim 1 - 2$ TeV, requiring $m_1 \geq m_\phi + m_\psi \gtrsim 3$ TeV.

WIMP Decay to Leptons and ADM (Sec. 2.3)

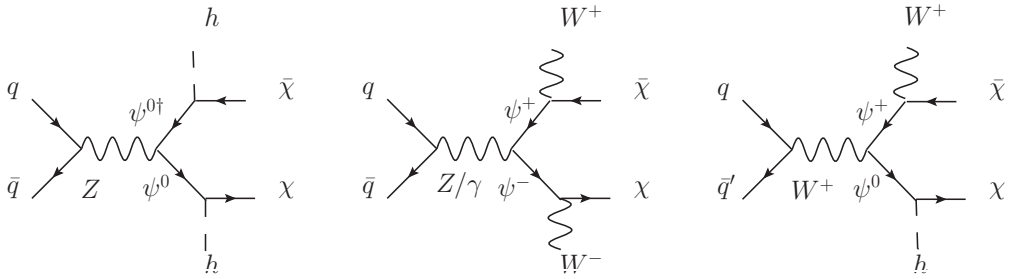

Figure 2.12: Diagrams relevant for ψ production at hadron colliders (WIMP cogenesis with leptons).

In this model, ϕ and ψ are both electroweak doublets. Thus at the LHC the neutral and charged components of these new states are produced through EW processes with intermediate W, Z bosons, and subsequently decay as $\psi^0 \to h\chi$, $\psi^\pm \to W^\pm\chi$, $\phi^\pm \to \ell^\pm\chi$, $\phi^0 \to \nu\chi$. Consequently, these lead to signals: of $\psi^0\psi^0 \to 4b(4j) + \not{E}_T$, $\psi^+\psi^- \to W^+W^- + \not{E}_T$, $\phi^+\phi^- \to 2\ell + \not{E}_T$, $\phi^0\phi^0 \to \not{E}_T$. The figures for these processes are shown in Figs. 2.12 and 2.13.

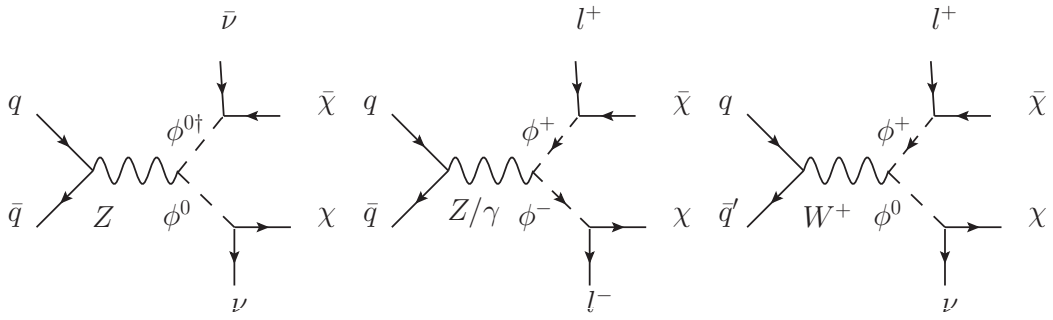

Figure 2.13: Diagrams relevant for ϕ searches at hadron colliders (WIMP cogenesis with leptons).

LHC searches for charginos $\tilde{\chi}^\pm$ and charged sleptons $\tilde{l}^\pm$ bound the charged components of ψ, and ϕ, respectively, while searches for heavier neutralinos $\tilde{\chi}_2^0$ bound the neutral component of ψ. Specifically, searches for $\tilde{\chi}^\pm \to W^\pm\tilde{\chi}_1^0$ produces the same collider signature as decaying $\psi^\pm$, $\tilde{\chi}_2^0 \to h\tilde{\chi}_1^0$ the same signature as decaying ψ^0, and $\tilde{l}^\pm \to l^\pm\tilde{\chi}_1^0$ the same signature as decaying $\phi^\pm$. Since we assume mass degeneracy among the different generations and components of ϕ and ψ, the relevant LHC searches are in the cases of $m_{\tilde{\chi}^\pm} = m_{\tilde{\chi}_2^0}$ and $m_{\tilde{e}} = m_{\tilde{\mu}} = m_{\tilde{\tau}}$.

At 13 TeV, ATLAS places bounds on the masses charginos and neutralinos with 139 fb^{-1} of data with $m_{\tilde{\chi}^\pm} = m_{\tilde{\chi}_2^0} \gtrsim 740$ GeV assuming massless LSP $\tilde{\chi}_1^0$ [91]. We apply

these bounds directly to the charged and neutral components of ψ: $m_{\psi^\pm} = m_{\psi^0} \gtrsim 740$ GeV. With the same set of data ATLAS places bounds on the masses of charged sleptons in the mass degenerate limit of $m_{\tilde{l}} \gtrsim 700$ GeV [92]. We apply these bounds directly to the charged components of ϕ: $m_\phi \gtrsim 700$ GeV.

Finally, note that just like in the earlier studied WIMP baryogenesis models [66,71], the long-lived WIMP, Y_1, in WIMP cogenesis (for both the quark and lepton models we presented) is also expected to leave distinctive displaced vertex signatures if it can be produced at a collider experiment (e.g. through $qq \to Z'^{(*)} \to Y_1 Y_1$). However, Y_1 is a SM singlet with typically O(TeV) mass which makes it hard to access with the LHC. Nevertheless it may be within reach of future high energy colliders (e.g. [93]) and leave spectacular signatures involving both displaced vertices (baryon asymmetry) and missing energy (ADM).

A complementary signal at colliders is possible via the S mixing with the SM Higgs through $S|H|^2$ or $S^2|H|^2$ [94]. This can lead to rare or invisible Higgs decay through $h \to SS$ [95–97]. The specifics of the signal channel depends on model details about $S - H$ interactions which is beyond the scope of this work.

2.4.2 Dark Matter Direct Detection

As expected in most of asymmetric DM models, since $\bar{\chi}$ is depleted to triviality in the early universe, indirect detection rates are negligible. Therefore we focus on the direct detection prospect of χ.

WIMP decay to baryons and ADM (Sec. 2.2)

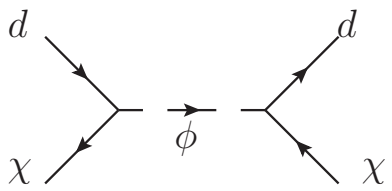

Figure 2.14: Dominant process contributing to $\chi N \to \chi N$ scattering.

The only available channel for χ to interact with quarks is $\chi d \to \chi d$ mediated by ϕ (shown in Fig. 2.14). By integrating out ϕ in the low energy effective theory, the effective DM-quark interaction operator is $\frac{\alpha_i^2}{m_\phi^2}(\bar{d}\chi)(\chi d)$, leading to spin-independent (SI) interactions between the DM and nucleon. These translate to contributions to a χ-nucleon effective interaction following [98]. The SI χ-nucleon cross section is

$$\sigma_{\rm SI}(\chi N \to \chi N) \approx \frac{1}{\pi}\left[\frac{m_\chi m_n}{m_\phi^2(m_\chi + m_n)}(0.26\alpha_s^2 - 0.967\alpha_d^2)\right]^2 \tag{2.26}$$

As we have seen, the DM mass in WIMP cogenesis model is predicted to be in the sub-GeV to GeV range. The strongest current limits on $\mathcal{O}$(GeV) SI DM-nucleon interactions come from DarkSide-50 [27]: for DM masses within 2-3 GeV, the upper limit on the DM-nucleon cross section is $5 - 7 \times 10^{-42}$ cm^2. In the case that the asymmetry is produced before the EWPT, the DM mass is below 1 GeV and the strongest bounds come from CRESST [99]. Specifically for DM masses of $0.5 - 1$ GeV, the upper limit on DM-nucleon scattering is between $\sigma_{SI} \sim 10^{-38} - 10^{-36}$ cm^2.

Now we give numerical examples from our model. With $\alpha_d = \alpha_s = 1$ and scalar mass at the lower bound provided by colliders, $m_\phi = 2$ TeV and $m_\chi = 2.5$ GeV, the SI

DM-nucleon cross section is $\sigma(\chi N \to \chi N) \approx 2 \times 10^{-42}$ cm^2. This is not only currently safe from the most stringent bound, but also within reach future iterations of DarkSide and other upcoming direct detection experiments [100–102]. In the case that $m_\chi = 0.89$ GeV, we again take $\alpha_s = \alpha_d = 1$ and scalar masses $m_\phi = 2$ TeV, we obtain a benchmark value from Eq. 2.26 of $\sigma_{\rm SI}(\chi N \to \chi N) \approx 1.02 \times 10^{-42}$ which is well below the bound set by CRESST but can be within reach of future searches for sub-GeV DM such as with the LUX-ZEPLIN [102].

WIMP Decay to Leptons and ADM (Sec. 2.3)

In this model, the dominant process for direct detection come from tree-level $\chi - e^-$ scattering via ϕ exchange. The diagram is identical to that for ADM-nucleon scattering in the quark model, with the quarks replaced with electrons. We can estimate the cross section for ADM-electron scattering by integrating out ϕ:

$$\sigma(\chi e^- \to \chi e^-) \approx \frac{1}{4\pi}\left(\frac{\alpha^2 m_\chi}{m_\phi^2}\right)^2 \tag{2.27}$$

Similar to WIMP cogenesis with quarks, the ADM mass is fixed by the ratio of DM to baryonic matter today. In our example model of WIMP cogenesis with leptons, the ADM mass is $m_\chi \approx 0.93 - 1.37$ GeV. For this mass range, Xenon100 constrains the cross-section of DM-scattering with electrons to be $\sigma_{SI} \lesssim 1 - 2 \times 10^{-37}$ cm^2 [101].

Owing to less stringent collider constraints, the masses of the intermediate states can be lighter in the model of WIMP cogenesis with leptons: $m_\phi,\ m_\psi \sim 700$ GeV. However, we need WIMP cogenesis to occur before the EWPT, when the temperature would be around or below $m_{\phi,\psi}$. Furthermore, the ADM annihilation to leptons is less constrained than annihilation to quarks [89] and we can have $\alpha > g$. Taking the benchmark parameters of

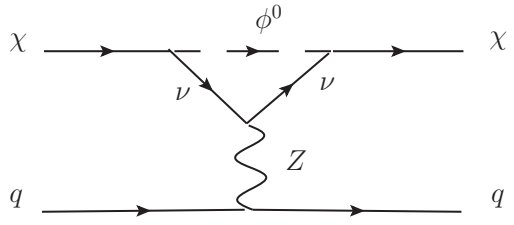

Figure 2.15: Loop diagram contributing to direct detection rate in WIMP cogenesis with leptons. There is another diagram contributing to $\chi q \to \chi q$ with the replacements $\phi^0 \to \phi^\pm$ and $\nu \to l^\pm$.

$m_\chi = 0.93{-}1.37$ GeV, $m_\phi = 700$ GeV and $\alpha = 1$ gives $\sigma(\chi e^- \to \chi e^-) \approx 1.1{-}2.4{\times}10^{-40}$ cm^2 which is just below the current bound by Xenon100 [101].

There are 1-loop processes in WIMP cogenesis with leptons (Fig. 2.15), that allow for our sub-GeV ADM to scatter with nucleons at direct detection experiments. However, the loop suppression combined with minimal bounds on sub-GeV DM scattering with nucleons makes the rate well below the sensitivity reach of foreseeable experiments.

2.4.3 Induced Nucleon Decay

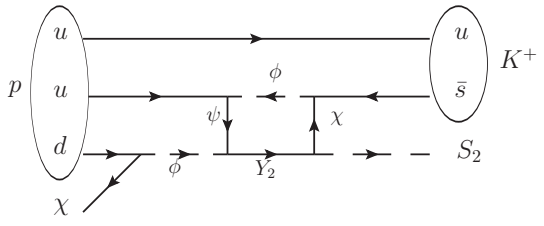

Figure 2.16: Potential induced nucleon decay signature arising in a model of WIMP cogenesis with baryons.

In the model presented in Sec. 2.2, a potential signal of B-violating (induced) nucleon decay is highly suppressed and undetectable with foreseeable experiments. However, an observable induced nucleon decay (IND) signature may arise with a minimal, well-motivated extension, for instance, by introducing an additional singlet scalar, S_2, with $m_{S_2} \lesssim$ GeV. With this introduction of S_2 comes a plethora of potential interactions. Of particular interest is the Yukawa interaction $\mathcal{L} \supset \gamma S_2 \bar{Y}_2 P_R \chi$ which then requires S_2 carry Z_4 charge i and generalized baryon number $G_{S_2} = 1/2$. This interaction, together with the set of interactions in Eq. 2.3 allows for the possibility of induced nucleon decay, as shown in Fig. 2.16. The analogous diagram with Y_1 is much more suppressed due to the very small η_1 to ensure a long lifetime of Y_1. S_2 can be a stable subdominant DM, or may decay, e.g. to S. The final decay channels from S_2 depend on model specifics beyond our minimal model, which we will defer for future consideration. Nevertheless a common feature is that for down-scattering processes, where $m_\chi > m_{S_2}$, the outgoing K meson momentum from IND will be larger than those resulting from standard nucleon decays. The IND event topology here resembles that in Hylogenesis [76] while this model is fully renormalizable.

The scattering process of $p+\chi \to K^+ + S_2$ proceeds via $\mathcal{O}_7 \sim \frac{\alpha^2 \beta \gamma \eta_2}{16\pi^2 m_2^3} S_2 (\bar{\chi} P_R d)(\bar{u} P_R d)$, and is estimated as:

$$\sigma(p + \chi \to S_2 + K^+) \sim \frac{1}{16\pi^3} \Big(\frac{\alpha^2 \beta \gamma \eta_2 m_p m_\chi}{m_2^3} \Big)^2$$

This leads to a prediction for the proton lifetime as $\tau_p^{-1} = n_{DM} \sigma(p + \chi \to S_2 + \pi^+) v$. This model gives τ_p consistent with the lower bound set by SuperKamiokande [103] but within reach of future experiments such as HyperKamiokande [104] and DUNE [105]. Our benchmark is: $m_\chi = 2.5$ GeV, $m_2 \sim 3$ TeV, and all couplings ~ 1 gives $\tau_p \sim 2 \times 10^{36}$ years.

2.4.4 Other Experimental Constraints

As discussed in the Model Setup (Sec. 2.2.1 and 2.3), new sources of FCNC are absent due to the $U(3)$ flavor symmetry of the model and thus the model is consistent with related constraints on FCNC. In addition, despite the presence of CP violation source necessary for the asymmetry generation, the model is exempt from the constraints on electric dipole moments (EDMs) for the neutron and electron [106, 107] . The reason is that, the interference diagrams (Fig. 2.5) leading to CP violation do not involve SM quarks or leptons, and the new fields couple exclusively to right-handed quarks or left-handed leptons.

WIMP cogenesis with baryons evades bounds from neutron-antineutron oscillation: the intrinsic interactions in the model and the $U(3)$ flavor symmetry together forbid $udd \to \bar{u}\bar{d}\bar{d}$ conversion at tree-level and 1-loop (alternatively with small couplings without invoking the flavor symmetry). Higher order process is strongly suppressed by loop factors and the TeV-scale masses of $Y_{1,2}$, ψ, and ϕ, even with $\mathcal{O}(1)$ couplings.

2.5 Darker Pieces to the Cosmological Triple Puzzle

There has been a proliferation of models which produce and thermalize DM in a sector hidden from the SM. These sectors are referred to as "hidden" because they may only interact with the SM through the gravitational interaction, other new states, or new symmetries. These models of hidden sector DM are well motivated: a simple explanation for DM's lack of detection is that it simply couples too feebly or not at all to the SM. A number of interesting mechanisms for populating and thermalizing a hidden sector of DM have been proposed [60, 108–110].

The unification of WIMP DM and ADM model-building frameworks accomplished by WIMP Cogenesis is but one appealing way of addressing the cosmological triple puzzle with minimal ambiguity. As we saw, a direct and unambiguous relationship was achieved through the production of a DM asymmetry. It would be particularly interesting if hidden sector production mechanisms can be used to connect a *symmetric* DM (DM=anti-DM) to the baryon asymmetry in a similarly unambiguous way. Using a multicomponent hidden sector, a stable, symmetric DM candidate can equilibrate to other, metastable states within the dark sector. These metastable states then decay to produce the baryon asymmetry. Our goal is to construct a viable model of *dark sector baryogenesis* with the following characteristics:

- Involves only renormalizable interactions;
- A multicomponent hidden sector consisting of states χ_i $(i \geq 3)$ decouples from the SM bath and equilibrates separately amongst themselves;
- The total number of states in the dark sector is conserved: $s * \sum_i Y_i = \text{constant}$;

The first characteristic can be found in the work discussed in the previous chapter [1] while the second characteristic is a generic feature of hidden sector models of DM. The third characteristic, among other things, distinguishes this model from other models which relate the baryon asymmetry to the DM abundance. The simplest version will consist of three hidden fermions $\chi_1,\ \chi_2,\ \chi_3$ where χ_1 is taken to be the stable DM candidate and χ_2 is the metastable component whose decays trigger baryogenesis. We assume, for simplicity, that χ_3 decays similarly to χ_2 but with larger mass and Yukawa couplings to quarks, such

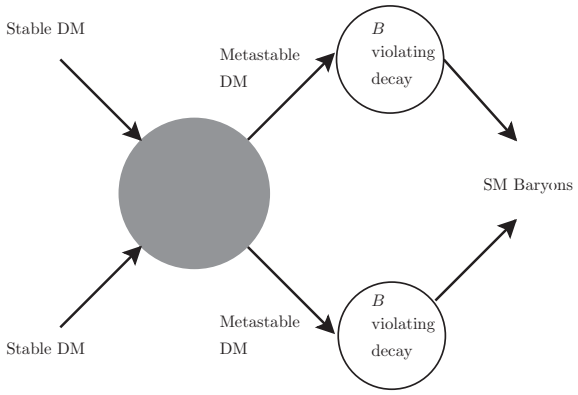

Figure 2.17: Schematic diagram showing freezeout of stable component via annihilations to metastable component whose decays produce the baryon asymmetry.

that it decays very early and in-equilibrium. It plays an important role in giving rise to a non-zero CP-asymmetry in χ_2 decays, in analogy to the role played by Y_2 and Y_1 in WIMP Cogenesis. When the metastable component eventually undergoes CP and baryon number violating decays, its abundance is converted into the baryon asymmetry. The basic idea is illustrated in the schematic of Fig. 2.17. The DM abundance and baryon asymmetry are established in three stages which satisfy the Sakharov conditions as follows

1. The hidden sector consisting decouples from the SM bath with roughly equal densities $Y_{\chi_1} \sim Y_{\chi_2}$. The hidden sector states equilibrate amongst themselves with temperature $T' \neq T_{\rm SM}$.

2. Processes $\chi_1\chi_2 \leftrightarrow \chi_2\chi_2$, which preserve the total number of χ_1 and χ_2, freezeout in the hidden sector. This step ensures a simple relation between the abundances $\Omega_{\chi_1} \approx \Omega_{\chi_2}$ while the freezeout ensures the out-of-equilibrium condition is satisfied.

3. C/CP- and B-violating decays of χ_2 to SM quarks. This step occurs well after the freezeout, but before BBN. The would-be abundance of χ_2 is transferred into a baryon asymmetry $\Omega_B \sim \epsilon_{CP}\Omega_{\chi_2}^{\tau\to\infty}$

2.5.1 Toy Model

In a concrete model, we require interactions which mediate the freezeout of both χ_1 and χ_2. Additionally, interactions which permit χ_2 decays must satisfy the Sakharov conditions. Since the departure from equilibrium condition is satisfied by the χ_1 and χ_2 freezeout, the interactions between χ_2 and the SM quarks must violate CP and baryon number. A Lagrangian which includes all of the necessary interactions is

$$\Delta\mathcal{L}_{\text{int}} = g\bar{\chi}_{1,2,3}i\gamma^5\chi_{1,2,3}S + \alpha_i\chi_2\bar{u}_i\phi + \beta_i\chi_3\bar{u}_i\phi + \eta_{ij}\phi d_i d_j + \text{h.c.} \tag{2.28}$$

The first term in Eq. 2.28 permits annihilations of $\chi_1\chi_1 \leftrightarrow \chi_2\chi_2$ mediated by SM singlet pseudoscalar S. The freezeout of these annihilations would establish the hidden sector abundances of χ_1 and χ_2 whose total number density would be conserved. The second and last terms permit the out-of-equilibrium decays $\chi_2 \to \phi^* u$ and $\phi \to dd$ with $\Delta B = 1$. CP-violation is achieved in χ_2 decays by the introduction of a third, heavier particle χ_3 with similar interactions to the SM as χ_2, which mediates interference between the tree and loop level diagrams shown in Fig. 2.18. The decays of χ_2 would trigger baryogenesis and the overall baryon asymmetry would be related to the χ_2 abundance by $\Omega_B \sim \epsilon_{CP}\Omega_{\chi_2}$. Because of the conservation of number density of total hidden sector states, the relic baryon asymmetry can be related to the relic abundance of χ_1.

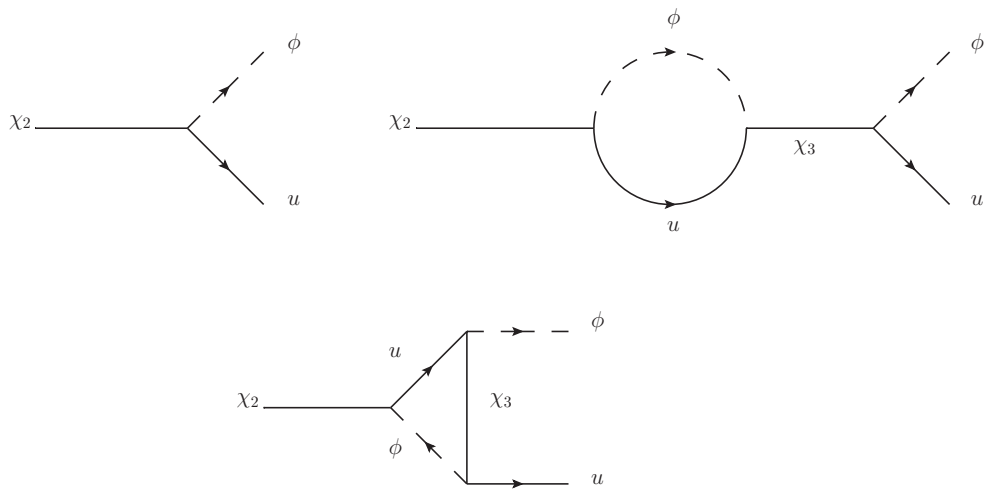

Figure 2.18: Diagrams contributing to CP violation in χ_2 decays

There are potential conventional and unique signature for the toy model introduced here. Since the stable species has no tree-level couplings to the SM, direct detection constraints are evaded while one-loop scattering permits detection at upcoming experiments. This mechanism permits peculiar indirect detection signatures as well. DM annihilations (χ_1) in the galactic center can produce metastable states (χ_2)which would produce detectable B-violating signatures at indirect detection experiments via χ_2 decays to SM baryons.

A number of other interesting mechanisms for populating and thermalizing the dark sector already exist [41, 111–113]. It will be very interesting to explore how these may be applied to producing the baryon asymmetry via the hidden sector and how the consequences for relating baryogenesis to the DM abundance may be different between these frameworks.

Part III

On the Nature of the Neutrino

Chapter 3

Unraveling the Dirac Neutrino with Cosmological and Terrestrial Detectors

3.1 Introduction

The phenomenon of neutrino flavor oscillations [14, 114–117] requires that at least two neutrinos are massive. However, the Standard Model (SM) predicts massless neutrinos [118], and therefore new physics is required to explain the origin of neutrino mass. Broadly speaking, neutrino mass models fall into two categories. The Majorana Neutrino Hypothesis (MNH) posits that neutrinos are their own antiparticles, and no new degrees of freedom are needed at the $O(m_\nu)$ scale [119]. On the other hand, the Dirac Neutrino Hypothesis (DNH) introduces three new degrees of freedom that combine with the SM neutrinos to form three Dirac pairs of particles and antiparticles [120]. The DNH can be viewed as the limit where the Majorana mass terms in the MNH are zero. If the neutrinos are Dirac particles, then for each "active" neutrino that we have measured, there must exist a *precisely degenerate* "sterile" neutrino partner. This limit is smooth, however: the quasi-Dirac (or "pseudo-Dirac") hypothesis (QDH) [121–124] is that in which small deviations from vanishing Majorana mass terms give rise to light gauge-singlet sterile Majorana neutrinos which are near degenerate in mass with the left-handed (active) neutrinos. Determining whether neutrinos are Majorana or Dirac is of utmost importance for advancing our understanding of these elementary particles.

In the minimal model, these sterile states are so weakly interacting that they are never produced in any significant abundance in the early universe [125, 126], and they do not leave a detectable imprint on cosmological observables. However, there are many compelling beyond the SM scenarios in which the sterile states acquire a thermal distribution in the early universe and survive today as cosmological relics. We demonstrate how this

leads to deviations in the cosmological neutrino observables (namely, $N_{\rm eff}$ and Σm_ν) that are correlated with one another, as expected in general for eV-scale relics [127], and also correlated with terrestrial neutrino observables (namely, m_{ν_e} and $\Sigma_i m_i$), as also pointed out recently in [62].

3.2 Models with thermal sterile neutrinos

In this section we discuss two examples in which Dirac neutrinos' sterile partners can reach a thermal or near-thermal abundance in the early universe: *Dirac leptogenesis* (LG) [128–134], which are motivated by explaining the observed baryon asymmetry using Dirac neutrinos, and models with gauged Baryon minus Lepton number (B-L) symmetry [135–139]. A gauged $U(1)_{B-L}$ is particularly desirable in excluding $\Delta L = 2$ Majorana mass terms, considering that their global symmetry counterpart may be undermined by quantum gravity [140, 141]. The $U(1)_{B-L}$ may be broken by $\Delta L > 2$ units for $m'_Z \neq 0$.

We begin by reviewing why new physics is required to yield a substantial population of steriles [125, 126]. The simplest way to implement the Dirac neutrino hypothesis is via the Yukawa interaction

$$\mathcal{L}_\nu = Y_\nu^{ij} \bar{L}^i \tilde{H} \nu_R^j + \text{h.c.} \tag{3.1}$$

where $L = (\nu_L, e^-)$ is the left-handed lepton doublet, H is the Higgs doublet, ν_R is the right-handed sterile neutrino, and Y_ν^{ij} is the matrix of Yukawa couplings. After electroweak symmetry breaking, ν_L and ν_R combine to give a Dirac fermion with mass $m_\nu \sim y_\nu v_{\rm ew}$. Taking $m_\nu \sim 0.1$ eV requires $y_\nu \sim 10^{-12}$. Since this tiny Yukawa coupling is the sole

interaction with the SM, the ν_R do not come into thermal equilibrium. Nevertheless, thermal freeze-in [142] (see also [143]) generates ν_R out of equilibrium via reactions such as $e^-\nu_L \to e^-\nu_R$ when the plasma temperature is $T \sim T_{ew} \sim 100$ GeV. The predicted abundance is parametrically $\Omega_{\nu_R} \sim \rho_{\nu_R}/T_{ew}^4 \sim \langle\sigma v\rangle n_e n_{\nu_L}/HT_{ew}^3 \sim G_F^2 m_\nu^2 T_{ew} M_{\rm pl}$ where $\langle\sigma v\rangle \sim G_F^2 m_\nu^2$ is the thermally-averaged production cross section, $n_e \sim n_{\nu_L} \sim T_{ew}^3$ is the electron density, $H \sim T_{ew}^2/M_{\rm pl}$ is the Hubble expansion rate, and $M_{\rm pl} \simeq 2.43 \times 10^{18}$ GeV is the reduced Planck mass. Putting in numbers gives $\Omega_{\nu_R} \sim 10^{-8}\,(m_\nu/0.1\text{ eV})^2$, which corresponds to an undetectably small population. Thus if the neutrinos are Dirac and contribute detectably to the relativistic energy density in the early universe, physics beyond the SM is required.

In Dirac LG models, a new $SU(2)_L$ scalar doublet Φ decays out-of-equilibrium, and produce equal and opposite asymmetries of ν_R and ν_L. These ν_R and ν_L are kept in thermal equilibrium in the early Universe through the scattering process mediated by Φ. Nevertheless in order to avoid washing out the asymmetries produced in ν_R and ν_L, these processes need to depart from equilibrium before, or around the time when Dirac LG is triggered by Φ decay. The exact time of Φ decay is model-dependent, but generally has to be before the electro-weak phase transition (EWPT) so that sphalerons can convert the lepton asymmetry to a baryon asymmetry. Therefore we find that $T_{\rm dec}$ should satisfy $T_{\rm dec} \gtrsim T_{\rm EWPT}$ and $\Delta N_{\rm eff} \sim 0.05{-}0.14$, depending on the number of new particles introduced in the model (e.g. whether in the framework of MSSM [129] or not [128, 132]).

In gauged B-L models, interactions mediated by Z' gauge bosons thermalize ν_R with the SM plasma via s-channel processes such as $f\bar{f} \leftrightarrow \nu_R\bar{\nu}_R$. The decoupling of ν_R occurs below the $U(1)_{B-L}$ breaking scale. By comparing the interaction rate $\Gamma_s \sim$

$g'^4 T^5/m_{Z'}^4$ and the Hubble expansion rate, we find the decoupling temperature $T_{\rm dec} \lesssim (m_{Z'}/g' M_{\rm pl})^{4/3} M_{\rm pl}$. Because these models extend the SM by up to three ν_R and Z' the total effective number of d.o.f can be as large as $g_*(T_{\rm dec}) \approx 115$ and as low as $g_*(T_{\rm dec}) \approx 75.25$, which translates to $\Delta N_{\rm eff} \approx 0.13 - 0.23$.

Additionally, a number of Dirac neutrino models are motivated by generating small neutrino masses through inclusion of additional Higgs doublets or mediator mass/loop suppression [62,144–148]. Thus there are many reasons to expect abundantly populated and thermalized sterile neutrinos in the early universe. These sterile neutrinos would interact more weakly relative to their active counterparts and necessarily decouple earlier.

3.3 Terrestrial and cosmological probes of neutrinos

Efforts are underway in the lab to measure the absolute neutrino mass scale. This can be parametrized by the effective electron neutrino mass, $m_{\nu_e} = [\sum_i m_i^2 |U_{ei}|^2]^{1/2}$, where U_{ei} is the neutrino mixing matrix [120]. We are also interested in the sum of the three active neutrino masses, $\Sigma_i m_i \equiv m_{\nu_1} + m_{\nu_2} + m_{\nu_3}$, which can be determined from the measured m_{ν_e} by knowing the squared mass splittings, the mixing angles, and mass ordering [120]. We choose to infer $\Sigma_i m_i$ this way as the direct measurement of m_{ν_μ} or m_{ν_τ} has sensitivity of $O(0.1 - 10)$ MeV which is much worse than the related sensitivity from cosmological observations [149,150]. At present, the best experimental technique uses precision measurements of the tritium beta decay endpoint. Since a beta decay produces

an (anti-)neutrino, which carries away an energy of at least $O(m_{\nu_e})$, the endpoint of the electron spectrum shifts downward for larger neutrino mass. Currently the best limits come from the KATRIN experiment [4], which measures an effective neutrino mass squared value of $m^2_{\nu_e} = (-1.0^{+0.9}_{-1.1})$ eV^2, corresponding to an upper limit of $m_{\nu_e} < 1.1$ eV (90% CL) [7]. As a constraint on the absolute neutrino mass scale, this is roughly $\Sigma_i m_i \lesssim 3$ eV. With more data, KATRIN is expected to constrain $m_{\nu_e} < 0.2$ eV (90% C.L.) or measure the absolute neutrino mass (5σ) if it is larger than $m_{\nu_e} = 0.35$ eV [5], corresponding to $\Sigma_i m_i = 1.05$ eV (same for either normal or inverted mass ordering). Concurrently the Project 8 experiment is under construction, and it aims to achieve a neutrino mass sensitivity at the level of $m_{\nu_e} = 0.04$ eV (90% C.L.) [6], which corresponds to $\Sigma_i m_i = 0.14$ eV in the normally-ordered neutrino mass spectrum, and 0.099 eV in the inverted one.

At the same time, cosmological probes of relic neutrinos are becoming increasingly sensitive. During the epochs of Big Bang nucleosynthesis (BBN) and baryon acoustic oscillations (BAO), neutrinos were relativistic, and their effect on cosmology is primarily through $N_{\rm eff}$. In particular, the presence of the sterile states allows $N_{\rm eff} > N^{(0)}_{\rm eff}$. A larger $N_{\rm eff}$ implies a larger radiation energy density, and therefore a larger Hubble parameter H. During BBN, this changes the relationship between the expansion rate, H, and the temperature of the standard model plasma, and thus $N_{\rm eff}$ at $T \sim 0.1$ MeV can be inferred from the primordial elemental abundances [151]. At recombination, a larger expansion rate increases the angular scale of diffusion damping as compared with the acoustic scale, $\theta_d/\theta_s \sim H^{1/2}$ [152], and so $N_{\rm eff}$ at $T \sim 0.1$ eV can be inferred from measurements of the CMB power spectrum at small angular scales (high ℓ). In particular, because neutrinos free-

stream, they lead to a unique phase-shift of the CMB's acoustic peaks [153] that has now been detected [154]. Currently, Planck restricts $\Delta N_{\rm eff} < 0.3$ (95% C.L.) [8]. The constraint is slightly loosened if ν_R is interacting [60, 155, 156] which is possible, *e.g.*, in the gauged $U(1)_{B-L}$ scenario. Future surveys, such as CMB Stage-IV, will constrain $\Delta N_{\rm eff} \lesssim 0.06$ (95% C.L.) [157, 158]. The CMB power spectra also rule out neutrinos that become non-relativistic around recombination, and require that each flavor of active neutrino satisfies $m_\nu < 1$ eV [8].

At late times, the neutrinos became nonrelativistic, and their energy density can be parametrized by $\Omega_\nu h^2 = \Sigma_i m_{\nu_i} n_{\nu_i}/(3M_{\rm pl}^2 H_{100}^2) \equiv \Sigma m_\nu/94$ eV where $H_{100} = 100$km/sec/Mpc, and this defines the effective neutrino mass sum, Σm_ν. These cold neutrinos are free streaming on the scale $l_{\rm fs} \approx (250{\rm Mpc})(m_\nu/{\rm eV})^{-1}$ [159]. This suppresses the growth of structure, which leads to less lensing in the CMB and less structure today, probed by Lyman-α forest and BAO surveys. In particular, measurements of the gravitational lensing of the CMB as well as measurements of galaxy clustering are sensitive to the sum of the neutrino masses. This effect has not yet been observed, and future surveys will greatly increase the sensitivity [157].

A combination of CMB and large-scale structure (LSS) surveys put a strong upper bound on Σm_ν [160]. The value of this bound is model dependent. For the 7-parameter model in which ΛCDM is extended by Σm_ν alone, a combination of Planck (temperature, polarization, lensing) and BAO gives $\Sigma m_\nu < 0.12$ eV (95% C.L.) [8]. If the neutrino mass scale obeys the strong constraint, $\Sigma_i m_i \leq \Sigma m_\nu < 0.12$ eV, then beta decay experiments like KATRIN will be unable to provide a laboratory measurement of the absolute neutrino mass

scale. However, the cosmological limits are model dependent, and going beyond the restrictive framework of ΛCDM gives more freedom. For instance, the extended-ΛCDM model (eΛCDM) [9] has up to 12 free parameters, including $N_{\rm eff}$, Σm_ν, the dark energy equation of state, and the running of the scalar spectral index. In these models, the inferred upper limit is much weaker $\Sigma m_\nu \lesssim 0.4$ eV (95% C.L.), and remains consistent with laboratory limits from KATRIN.

3.4 Correlated terrestrial and cosmological observables

Let us now derive a correlation between the cosmological neutrino observables, $N_{\rm eff}$ and Σm_ν, and the terrestrial neutrinos observable, $\Sigma_i m_i$. The result Eq. 3.7 appears in [62] without derivation. We present the derivation here, both for readers who are unfamiliar with cosmological relic calculations and to emphasize the special role played by the degeneracy of active and sterile neutrinos in the DNH. We show that this correlation arises if the neutrinos are Dirac and if there is a thermal population of the sterile states. See also [127] for a discussion of general eV-scale relics and their impact on cosmological observables, and see Refs. [49, 62] for a discussion of Dirac neutrinos in cosmology.

First we consider the relic background of active neutrinos. The active neutrinos were initially in thermal equilibrium with the primordial plasma, and they decoupled at a time $t_{a,\rm dec}$ when the scale factor was $a_{a,\rm dec} = a(t_{a,\rm dec})$ and the plasma temperature was $T_{a,\rm dec} = T(t_{a,\rm dec}) \simeq$ MeV. Since the neutrino masses are $\lesssim O(\text{eV})$, the active neutrinos were

relativistic at the time of decoupling. After decoupling, the active neutrinos cooled due to the cosmological expansion and their temperature decreased as $T_{a,\mathrm{dec}}\,[a(t)/a_{a,\mathrm{dec}}]^{-1}$. Eventually the active neutrinos became non-relativistic at a time $t_{a,\mathrm{nr}}$ when $a_{a,\mathrm{nr}} = a(t_{a,\mathrm{nr}})$ such that their mass can be related to the decoupling temperature by $m_a = T_{a,\mathrm{dec}}\,(a_{a,\mathrm{nr}}/a_{a,\mathrm{dec}})^{-1}$. The formulas here hold approximately as long as the mass splitting is smaller than the total mass, so that the three active neutrinos become non-relativistic within $O(1)$ Hubble times of one another. We can write the energy density in the active neutrinos as [161]

$$\rho_a \approx \begin{cases} 6\frac{7}{8}\frac{\pi^2}{30}T_{a,\mathrm{dec}}^4\left(\frac{a(t)}{a_{a,\mathrm{dec}}}\right)^{-4} & ,\ t_{a,\mathrm{dec}} < t < t_{a,\mathrm{nr}} \\ 2\frac{7}{8}\frac{\pi^2}{30}T_{a,\mathrm{dec}}^3\left(\frac{a(t)}{a_{a,\mathrm{dec}}}\right)^{-3}\Sigma_i m_i\,, & t_{a,\mathrm{nr}} < t \end{cases} \tag{3.2}$$

where the assumptions of instantaneous decoupling and non-relativistic transition introduce a $\lesssim O(1)$ uncertainty.

Next we turn our attention to the relic background of sterile neutrinos. We assume that the sterile neutrinos were once in thermal equilibrium with the plasma, and that they decoupled at a time $t_{s,\mathrm{dec}}$ such that $a_{s,\mathrm{dec}} = a(t_{s,\mathrm{dec}})$ and $T_{s,\mathrm{dec}} = T(t_{s,\mathrm{dec}})$. We are interested in $t_{s,\mathrm{dec}} < t_{a,\mathrm{dec}}$ and $T_{s,\mathrm{dec}} > T_{a,\mathrm{dec}} \simeq$ MeV so that the sterile neutrinos decoupled before the active neutrinos. In that case, they will not share the entropy injections from the decoupling of other Standard Model species, and we expect the sterile neutrinos to be colder than the active neutrinos at any given time. This means that the sterile neutrinos became nonrelativistic before the active neutrinos. Let $t_{s,\mathrm{nr}}$ be the time when the sterile neutrinos became non-relativistic with $a_{s,\mathrm{nr}} = a(t_{s,\mathrm{nr}})$ such that $m_s = T_{s,\mathrm{dec}}\,(a_{s,\mathrm{nr}}/a_{s,\mathrm{dec}})^{-1}$. Here we write the sum of sterile neutrino masses as $\Sigma_i m_{s,i}$, which must equal the sum of active neutrino masses $\Sigma_i m_i$ in the DNH, but the formulas written here also apply for a

more general eV-scale relic with $\Sigma m_{s,i} \neq \Sigma_i m_i$. Then the energy density of the sterile neutrinos is written as

$$\rho_s \approx \begin{cases} 6\frac{7}{8}\frac{\pi^2}{30}T_{s,\mathrm{dec}}^4\left(\frac{a(t)}{a_{s,\mathrm{dec}}}\right)^{-4} & ,\ t_{s,\mathrm{dec}} < t < t_{s,\mathrm{nr}} \\ 2\frac{7}{8}\frac{\pi^2}{30}T_{s,\mathrm{dec}}^3\left(\frac{a(t)}{a_{s,\mathrm{dec}}}\right)^{-3}\Sigma_i m_{s,i}\,, & t_{s,\mathrm{nr}} < t \end{cases} . \tag{3.3}$$

Note that $\rho_s \leq \rho_a$ since $T_{s,\mathrm{dec}}a_{s,\mathrm{dec}} \leq T_{a,\mathrm{dec}}a_{a,\mathrm{dec}}$.

The cosmological observables are N_{eff} and Σm_ν. We can write

$$N_{\mathrm{eff}} = \mathcal{K}_N\big(\rho_a + \rho_s\big)\big|_{t=t_{\mathrm{CMB}}},\ \Sigma m_\nu = \mathcal{K}_m\big(\rho_a + \rho_s\big)\big|_{t=t_0}, \tag{3.4}$$

where the numerical coefficients, $\mathcal{K}_N$ and $\mathcal{K}_m$, are independent of the mass hypothesis. It is also useful to define $N_{\mathrm{eff}}^{(0)}$ and $\Sigma m_\nu^{(0)}$ by setting $\rho_s = 0$ in 3.4. We know that $N_{\mathrm{eff}}^{(0)} \simeq 3.044$ counts the three active neutrino flavors [57, 58], and $\Sigma m_\nu^{(0)} = \Sigma_i m_i$ is the sum of the three active neutrino masses.

Now let us consider the ratios

$$\frac{N_{\mathrm{eff}}}{N_{\mathrm{eff}}^{(0)}} = 1 + \frac{\rho_s}{\rho_a}\Big|_{t=t_{\mathrm{CMB}}}\ , \quad \frac{\Sigma m_\nu}{\Sigma m_\nu^{(0)}} = 1 + \frac{\rho_s}{\rho_a}\Big|_{t=t_0}, \tag{3.5}$$

whose deviations from unity parametrize the effect of the sterile neutrinos. We evaluate these expressions using the formulas for ρ_a and ρ_s that appear above. We know that the active neutrinos are relativistic at t_{CMB} and that they are nonrelativistic at t_0. Since the sterile neutrinos are colder than the active ones, they must also be nonrelativistic at t_0. We *assume* that the sterile neutrinos are relativistic at t_{CMB}, which can be checked in a particular model for sterile neutrino production. Using Eqns. (3.2) and (3.3), we have

$$\begin{aligned} \frac{N_{\mathrm{eff}}}{N_{\mathrm{eff}}^{(0)}} &= 1 + \left(\frac{a_{s,\mathrm{dec}}T_{s,\mathrm{dec}}}{a_{a,\mathrm{dec}}T_{a,\mathrm{dec}}}\right)^4 \quad \text{and} \\ \frac{\Sigma m_\nu}{\Sigma m_\nu^{(0)}} &= 1 + \frac{\Sigma_i m_{s,i}}{\Sigma_i m_i}\left(\frac{a_{s,\mathrm{dec}}T_{s,\mathrm{dec}}}{a_{a,\mathrm{dec}}T_{a,\mathrm{dec}}}\right)^3 \end{aligned} \tag{3.6}$$

For a general eV-scale relic, the mass ratio $\Sigma_i m_{s,i}/\Sigma_i m_i$ may be different from unity, but if the eV-scale relics are the sterile (Dirac) partners to the active neutrinos, then we must have $\Sigma_i m_{s,i}/\Sigma_i m_i = 1$, and we find

$$\left(\frac{N_{\rm eff}}{3.044} - 1\right)^{1/4} = \left(\frac{\Sigma m_\nu}{\Sigma_i m_i} - 1\right)^{1/3} \tag{3.7}$$

This is the correlation that we set out to derive. An equivalent expression appears in [62].

To parameterize this expression, recall that the comoving entropy density at time t is $a(t)^3\, s(t) = (2\pi^2/45)\, g_{*S}(t)\, a(t)^3\, T(t)^3$, where $g_{*S}(t)$ is the effective number of relativistic species [161]. If the comoving entropy density is conserved between times $t_{s,\rm dec}$ and $t_{a,\rm dec}$, then we can write

$$\frac{a_{s,\rm dec} T_{s,\rm dec}}{a_{a,\rm dec} T_{a,\rm dec}} = \left(\frac{g_{*S}(t_{a,\rm dec})}{g_{*S}(t_{s,\rm dec})}\right)^{1/3}, \tag{3.8}$$

which is the ratio that appears in 3.6.

3.5 Results and discussion

The relation in 3.7 implies a correlation between the cosmological neutrino observables, $N_{\rm eff}$ and Σm_ν, and $\Sigma_i m_i$ as inferred from terrestrial observable m_{ν_e}. We plot this relation in 3.1, along with various benchmark points derived using 3.8. Recall that $g_{*S}(t_{a,\rm dec}) \approx 10.75$ is the effective number of relativistic species when the active neutrinos decouple near $T_{a,\rm dec} \simeq 1$ MeV, and it is $g_{*S}(t_{s,\rm dec}) > 10.75$ when the sterile neutrinos decouple. If $g_{*S}(t_{s,\rm dec}) \gg g_{*S}(t_{a,\rm dec})$ then the sterile neutrinos are much colder than the

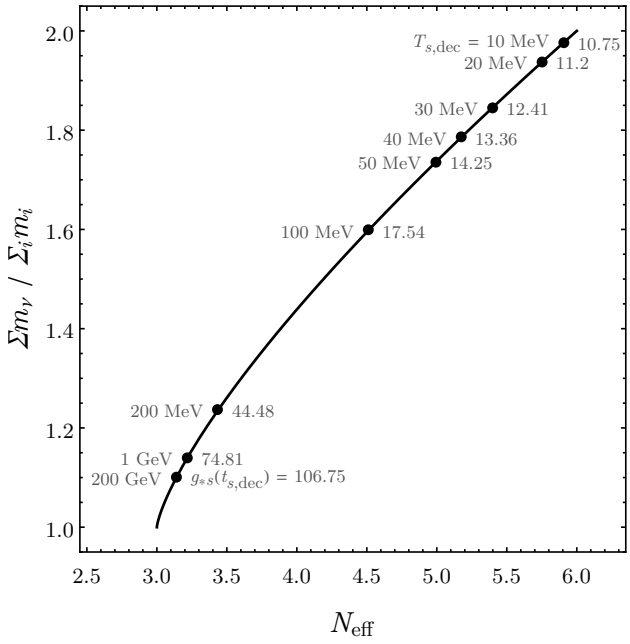

Figure 3.1: The effective number of neutrino species N_{eff} and the effective sum of neutrino masses Σm_ν are related through 3.7. Each point along the curve corresponds to a different decoupling temperature for the sterile neutrinos $T_{s,\mathrm{dec}}$ (marked on the left side of the curve), which is also parametrized by g_{*S} at that time [3] (marked on the right side of the curve).

active ones at any given time, implying $N_{\mathrm{eff}} \approx 3.044$ and $\Sigma m_\nu \approx \Sigma_i m_i$. Alternatively if $g_{*S}(t_{s,\mathrm{dec}}) \approx g_{*S}(t_{a,\mathrm{dec}})$ then the sterile neutrinos decouple at almost the same time as the active ones, implying $N_{\mathrm{eff}} \approx 6.088$ and $\Sigma m_\nu \approx 2\Sigma_i m_i$. As detailed in Sec. 2, BSM scenarios posit new interactions for eV-scale sterile neutrinos which would allow them to decouple later and contribute to N_{eff}. In particular, in the most optimistic models of Dirac LG and gauged $B - L$ which predict additional contributions to N_{eff} as large as $\Delta N_{\mathrm{eff}} \approx 0.14$. According to the correlation of 3.7, these models would also contribute to Σm_ν that would lie on the curve in 3.1 with $\Sigma m_\nu \approx 1.15$.

In 3.2 we show a parameter space in which the effective neutrino mass sum, Σm_ν, and the effective electron-type neutrino mass, m_{ν_e}, are varied. We overlay curves of constant

$\Sigma m_\nu/\Sigma_i m_i$ from 1 to 2, which also correspond to constant $N_{\rm eff}$ from 3.044 to 6.088 through 3.7. The mapping from m_{ν_e} to $\Sigma_i m_i$ depends on the neutrino mass hierarchy, and we show both normal ordering (red) and inverted ordering (blue). The curve labeled $\Sigma m_\nu/\Sigma_i m_i = 1$ [and $N_{\rm eff} \approx 3$ from 3.7] corresponds to the "standard" prediction in which only the active neutrinos are present as cosmological relics, whereas the curves with $\Sigma m_\nu/\Sigma_i m_i > 1$ [and $N_{\rm eff} \gtrsim 3$ from 3.7] represent the predictions of the DNH with a once-thermalized population of sterile partners. The curves terminate at a point (indicated by a dot) where the lightest neutrino mass is vanishing. If the neutrino masses are very hierarchical, the connection with $N_{\rm eff}$ in 3.7 holds as long as the three flavors of sterile neutrino decouple at the same temperature as one another, but at higher temperature than that of the three flavors of active neutrinos.

Future cosmological surveys will have much greater sensitivity to $N_{\rm eff}$ and Σm_ν, while next-generation neutrino experiments aim to deliver a precision measurement of m_{ν_e} and $\Sigma_i m_i$. How will this data inform our understanding of neutrinos and their role in cosmology? If these experiments discover that $N_{\rm eff} \gtrsim 3.044$ and $\Sigma m_\nu \gtrsim \Sigma_i m_i$, this would provide strong evidence for the presence of a new cosmological relic with mass $m = O(0.1)$ eV [127]. What are the candidates for this eV-scale relic and how can we distinguish them with laboratory tests? The coincidence of m and $m_\nu = O(0.1)$ eV suggests a specific connection between the new relic and the known active neutrinos.

In this work, we have argued that the Dirac neutrino hypothesis provides a compelling explanation for eV-scale relics if there is a thermal population of sterile neutrinos. This hypothesis makes a clear and testable prediction [62], as it requires $N_{\rm eff}$, Σm_ν, and

$\Sigma_i m_i$ to obey 3.7. In the case of a general eV-scale relic, 3.7 remains valid but retains a factor of $(\Sigma_i m_i / \Sigma_i m_{s,i})^{1/3}$ on the right-hand side. In particular, if any correlation between $N_{\rm eff}$ and Σm_ν is observed, the different dependence on the sum of active neutrino masses between these cases can be used to distinguish the DNH from other types of eV-scale relics.

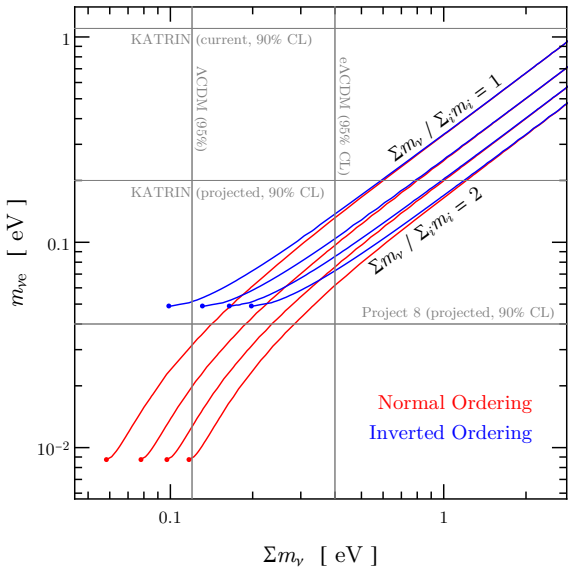

Figure 3.2: The effective sum of neutrino masses Σm_ν and the effective electron-type neutrino mass m_{ν_e} are shown here with overlaid curves corresponding to different values of $\Sigma m_\nu / \Sigma_i m_i = 1.00, 1.33, 1.66$ and 2.00. KATRIN and Project 8 sensitivities are taken from Refs. [4–7], while the model-dependent cosmological constraints are taken from Refs. [8, 9]. The red and blue curves correspond to the normal and inverted mass ordering, respectively, and the regime where they merge (upper-right corner) corresponds to the quasi-degenerate regime.

Part IV

Conclusions

Chapter 4

Conclusions

The SM does not appear to tell the full story of what particles make up the universe and how they interact. As outlined in the introduction, new physics is needed to explain the asymmetry of baryons over anti-baryons, the nature and origin of dark matter, and the origin of neutrino masses. In this thesis, the possibility that these conundrums are related and thus can be addressed by unified physical mechanisms is explored.

In Part II of this thesis, models are introduced to address the cosmological triple puzzle by connecting the baryon asymmetry to the dark matter abundance with shared interactions. In Chapter 2, we proposed WIMP cogenesis, a novel mechanism which addresses the *cosmological triple puzzle* about cosmic matter abundance in a unified framework: asymmetric dark matter and a baryon or lepton asymmetry are simultaneously generated from the same decay chain of a freezeout population of metastable WIMPs. The WIMP plays the role of grandparent for the matter abundance in the Universe, meanwhile the "coincidence" between DM and baryon abundances is automatically addressed via their co-production.

Additionally, the WIMP decay chain readily permits DM and baryon asymmetries to inherit a generalized WIMP miracle. The three Sakharov conditions are satisfied in three subsequent stages in order. ADM and baryons (leptons) share a generalized baryon (lepton) number symmetry that is conserved. We present two renormalizable models as benchmark examples realizing the idea, and find that with perturbative couplings and weak-scale masses for the new states, the observed DM and baryon relic densities can be explained while being compatible with relevant constraints. The models neatly predict ADM with mass $m_{DM} \sim 0.7 - 2.5$ GeV. These models can lead to testable signatures at a variety of experiments, including (low mass) DM direct detection, nucleon decay and the production of new SM charged particles at the LHC. Furthermore the long-lived WIMP in these models may be accessible with future high energy colliders, leaving spectacular signals by reproducing the cogenesis of matter in the early Universe.

At the end of Chapter 2, we introduce ongoing work on a mechanism of dark sector baryogenesis. The first stage of this process occurs when a dark sector composed of dark sector states χ_i ($i \geq 3$) decouple from the SM bath in the high temperature universe. These states equilibrate amongst themselves, separately from the SM bath, with $2 \leftrightarrow 2$ interactions and the constraint that their total number densities are conserved: $s * \sum_i Y_{\chi_i} = \text{constant}$. Eventually, these interactions freeze out which establishes a hidden sector DM abundance of one species. The conservation constraint then relates the abundance of the stable species to the abundances of the now out-of-equilibrium species which are metastable. These unstable species decay to SM quarks violate CP and baryon number and is transformed into the observed baryon asymmetry. Since this baryon asymmetry is directly related to the would-

be metastable abundance, which is in-turn directly related to the abundance of the stable species, the baryon asymmetry can be related to the stable species abundance. Thus, this mechanism permits a solution to the cosmological triple puzzle with symmetric DM candidates.

In Part III (Chapter 3), a test for distinguishing the neutrino as a Dirac fermion is outlined. In this work, we have argued that the Dirac neutrino hypothesis provides a compelling explanation for eV-scale relics if there is a thermal population of sterile neutrinos. The thermal population of Dirac neutrinos would have to be established through new physics Dirac leptogenesis or $U(1)_{B-L}$ models which seek to explain the matter-antimatter asymmetry, neutrino mass, and/or dark matter. This hypothesis makes a clear and testable prediction [62], as it requires $N_{\rm eff}$, Σm_ν, and $\Sigma_i m_i$ to obey 3.7. These measurements would provide strong evidence for a thermal population of relic sterile neutrinos. Laboratory efforts to directly detect the relic neutrino background [162, 163] could also uncover the presence of the sterile neutrinos [50, 51, 164, 165], providing an additional handle on this scenario. When the terrestrial and cosmological observables are taken together, they could be used to confirm the Dirac neutrino hypothesis.

Bibliography

[1] Yanou Cui and Michael Shamma. Wimp cogenesis for asymmetric dark matter and the baryon asymmetry. *Journal of High Energy Physics*, 2020(12), Dec 2020.

[2] Peter Adshead, Yanou Cui, Andrew J. Long, and Michael Shamma. Unraveling the dirac neutrino with cosmological and terrestrial detectors, 2020.

[3] Lars Husdal. On Effective Degrees of Freedom in the Early Universe. *Galaxies*, 4(4):78, 2016.

[4] A. Osipowicz et al. KATRIN: A Next generation tritium beta decay experiment with sub-eV sensitivity for the electron neutrino mass. Letter of intent. 9 2001.

[5] J. Angrik et al. KATRIN design report 2004. 2 2005.

[6] Ali Ashtari Esfahani et al. Determining the neutrino mass with cyclotron radiation emission spectroscopy—Project 8. *J. Phys. G*, 44(5):054004, 2017.

[7] M. Aker et al. Improved Upper Limit on the Neutrino Mass from a Direct Kinematic Method by KATRIN. *Phys. Rev. Lett.*, 123(22):221802, 2019.

[8] N. Aghanim et al. Planck 2018 results. VI. Cosmological parameters. 7 2018.

[9] Eleonora Di Valentino, Alessandro Melchiorri, and Joseph Silk. Beyond six parameters: extending ΛCDM. *Phys. Rev. D*, 92(12):121302, 2015.

[10] R. Aaij, B. Adeva, M. Adinolfi, C. Adrover, A. Affolder, Z. Ajaltouni, J. Albrecht, F. Alessio, M. Alexander, S. Ali, and et al. Measurement of form-factor-independent observables in the decay $b0 \to k0\mu + \mu-$. *Physical Review Letters*, 111(19), Nov 2013.

[11] A. Hicheur. Lhcb: Status and prospects on the b anomalies, 2021.

[12] James M. Cline. Baryogenesis. In *Les Houches Summer School - Session 86: Particle Physics and Cosmology: The Fabric of Spacetime*, 9 2006.

[13] Katherine Freese. Status of dark matter in the universe. *International Journal of Modern Physics D*, 26(06):1730012, Mar 2017.

[14] Y. Fukuda et al. Evidence for oscillation of atmospheric neutrinos. *Phys. Rev. Lett.*, 81:1562–1567, 1998.

[15] N. Aghanim et al. Planck 2018 results. VI. Cosmological parameters. 2018.

[16] Edward W. Kolb and Michael S. Turner. The Early Universe. *Front. Phys.*, 69:1–547, 1990.

[17] Laurent Canetti, Marco Drewes, and Mikhail Shaposhnikov. Matter and antimatter in the universe. *New Journal of Physics*, 14(9):095012, Sep 2012.

[18] A. D. Sakharov. Violation of CP Invariance, C asymmetry, and baryon asymmetry of the universe. *Pisma Zh. Eksp. Teor. Fiz.*, 5:32–35, 1967. [Usp. Fiz. Nauk161,no.5,61(1991)].

[19] James M. Cline. Is electroweak baryogenesis dead? *Phil. Trans. Roy. Soc. Lond. A*, 376(2114):20170116, 2018.

[20] Antonio Riotto. Theories of baryogenesis. In *ICTP Summer School in High-Energy Physics and Cosmology*, 7 1998.

[21] Michael Dine and Alexander Kusenko. Origin of the matter-antimatter asymmetry. *Reviews of Modern Physics*, 76(1):1–30, Dec 2003.

[22] V. C. Rubin, Jr. Ford, W. K., and N. Thonnard. Rotational properties of 21 SC galaxies with a large range of luminosities and radii, from NGC 4605 (R=4kpc) to UGC 2885 (R=122kpc). *Astrophys. J*, 238:471–487, June 1980.

[23] W. J. G. de Blok, Stacy S. McGaugh, Albert Bosma, and Vera C. Rubin. Mass density profiles of low surface brightness galaxies. *The Astrophysical Journal*, 552(1):L23–L26, May 2001.

[24] C. L. Bennett, D. Larson, J. L. Weiland, N. Jarosik, G. Hinshaw, N. Odegard, K. M. Smith, R. S. Hill, B. Gold, M. Halpern, and et al. Nine-year wilkinson microwave anisotropy probe (wmap) observations: Final maps and results. *The Astrophysical Journal Supplement Series*, 208(2):20, Sep 2013.

[25] Joel R. Primack. Dark matter and structure formation. In *Midrasha Mathematicae in Jerusalem: Winter School in Dynamical Systems*, 7 1997.

[26] Ortwin E. Gerhard and David N. Spergel. Dwarf Spheroidal Galaxies and the Mass of the Neutrino. *Astrophys. J*, 389:L9, April 1992.

[27] P. Agnes et al. Low-Mass Dark Matter Search with the DarkSide-50 Experiment. *Phys. Rev. Lett.*, 121(8):081307, 2018.

[28] Gianfranco Bertone, Nassim Bozorgnia, Jong Soo Kim, Sebastian Liem, Christopher McCabe, Sydney Otten, and Roberto Ruiz de Austri. Identifying WIMP dark matter from particle and astroparticle data. *JCAP*, 1803:026, 2018.

[29] Vasiliki A. Mitsou. Overview of searches for dark matter at the LHC. *J. Phys. Conf. Ser.*, 651(1):012023, 2015.

[30] S. Nussinov. TECHNOCOSMOLOGY: COULD A TECHNIBARYON EXCESS PROVIDE A 'NATURAL' MISSING MASS CANDIDATE? *Phys. Lett.*, 165B:55–58, 1985.

[31] Stephen M. Barr, R. Sekhar Chivukula, and Edward Farhi. Electroweak Fermion Number Violation and the Production of Stable Particles in the Early Universe. *Phys. Lett.*, B241:387–391, 1990.

[32] David B. Kaplan. A Single explanation for both the baryon and dark matter densities. *Phys. Rev. Lett.*, 68:741–743, 1992.

[33] David E. Kaplan, Markus A. Luty, and Kathryn M. Zurek. Asymmetric Dark Matter. *Phys. Rev.*, D79:115016, 2009.

[34] Kathryn M. Zurek. Asymmetric Dark Matter: Theories, Signatures, and Constraints. *Phys. Rept.*, 537:91–121, 2014.

[35] Kalliopi Petraki and Raymond R. Volkas. Review of asymmetric dark matter. *Int. J. Mod. Phys.*, A28:1330028, 2013.

[36] Jonathan L Feng, Huitzu Tu, and Hai-Bo Yu. Thermal relics in hidden sectors. *Journal of Cosmology and Astroparticle Physics*, 2008(10):043, Oct 2008.

[37] Lotty Ackerman, Matthew R. Buckley, Sean M. Carroll, and Marc Kamionkowski. Dark matter and dark radiation. *Physical Review D*, 79(2), Jan 2009.

[38] Zackaria Chacko, Yanou Cui, Sungwoo Hong, and Takemichi Okui. Hidden dark matter sector, dark radiation, and the cmb. *Phys. Rev. D*, 92:055033, Sep 2015.

[39] John Preskill, Mark B. Wise, and Frank Wilczek. Cosmology of the Invisible Axion. *Phys. Lett. B*, 120:127–132, 1983.

[40] Leanne D Duffy and Karl van Bibber. Axions as dark matter particles. *New Journal of Physics*, 11(10):105008, Oct 2009.

[41] Duccio Pappadopulo, Joshua T. Ruderman, and Gabriele Trevisan. Dark matter freeze-out in a nonrelativistic sector. *Physical Review D*, 94(3), Aug 2016.

[42] David N. Spergel and Paul J. Steinhardt. Observational evidence for selfinteracting cold dark matter. *Phys. Rev. Lett.*, 84:3760–3763, 2000.

[43] Ayuki Kamada, Manoj Kaplinghat, Andrew B. Pace, and Hai-Bo Yu. How the Self-Interacting Dark Matter Model Explains the Diverse Galactic Rotation Curves. *Phys. Rev. Lett.*, 119(11):111102, 2017.

[44] Sean Tulin and Hai-Bo Yu. Dark Matter Self-interactions and Small Scale Structure. *Phys. Rept.*, 730:1–57, 2018.

[45] K. Eguchi, S. Enomoto, K. Furuno, J. Goldman, H. Hanada, H. Ikeda, K. Ikeda, K. Inoue, K. Ishihara, W. Itoh, and et al. First results from kamland: Evidence for reactor antineutrino disappearance. *Physical Review Letters*, 90(2), Jan 2003.

[46] M. H. Ahn, E. Aliu, S. Andringa, S. Aoki, Y. Aoyama, J. Argyriades, K. Asakura, R. Ashie, F. Berghaus, H. G. Berns, and et al. Measurement of neutrino oscillation by the k2k experiment. *Physical Review D*, 74(7), Oct 2006.

[47] Stefano Dell'Oro, Simone Marcocci, Matteo Viel, and Francesco Vissani. Neutrinoless double beta decay: 2015 review. *Adv. High Energy Phys.*, 2016:2162659, 2016.

[48] J. Schechter and J. W. F. Valle. Neutrinoless double-beta decay in SU(2) x U(1) theories. *Phys. Rev.*, D25:2951, 1982.

[49] Keith A. Olive and Michael S. Turner. Cosmological Bounds on the Masses of Stable, Right-handed Neutrinos. *Phys. Rev. D*, 25:213, 1982.

[50] Mu-Chun Chen, Michael Ratz, and Andreas Trautner. Nonthermal cosmic neutrino background. *Phys. Rev. D*, 92(12):123006, 2015.

[51] Jue Zhang and Shun Zhou. Relic Right-handed Dirac Neutrinos and Implications for Detection of Cosmic Neutrino Background. *Nucl. Phys. B*, 903:211–225, 2016.

[52] Xuheng Luo, Werner Rodejohann, and Xun-Jie Xu. Dirac neutrinos and $N_{\rm eff}$. *JCAP*, 06:058, 2020.

[53] Debasish Borah, Arnab Dasgupta, Chayan Majumdar, and Dibyendu Nanda. Observing left-right symmetry in the cosmic microwave background. *Phys. Rev. D*, 102:035025, Aug 2020.

[54] Nickolay Y. Gnedin and Oleg Y. Gnedin. Cosmological neutrino background revisited. *Astrophys. J.*, 509:11–15, 1998.

[55] Gianpiero Mangano, Gennaro Miele, Sergio Pastor, Teguayco Pinto, Ofelia Pisanti, and Pasquale D. Serpico. Relic neutrino decoupling including flavor oscillations. *Nucl. Phys.*, B729:221–234, 2005.

[56] E. Grohs, G. M. Fuller, C. T. Kishimoto, M. W. Paris, and A. Vlasenko. Neutrino energy transport in weak decoupling and big bang nucleosynthesis. *Phys. Rev.*, D93(8):083522, 2016.

[57] Kensuke Akita and Masahide Yamaguchi. A precision calculation of relic neutrino decoupling. *JCAP*, 2008:012, 2020.

[58] Miguel Escudero Abenza. Precision Early Universe Thermodynamics made simple: $N_{\rm eff}$ and Neutrino Decoupling in the Standard Model and beyond. *JCAP*, 2005:048, 2020.

[59] Christopher Brust, David E. Kaplan, and Matthew T. Walters. New Light Species and the CMB. *JHEP*, 12:058, 2013.

[60] Zackaria Chacko, Yanou Cui, Sungwoo Hong, and Takemichi Okui. Hidden dark matter sector, dark radiation, and the CMB. *Phys. Rev. D*, 92:055033, 2015.

[61] Peter Adshead, Yanou Cui, and Jessie Shelton. Chilly Dark Sectors and Asymmetric Reheating. *JHEP*, 06:016, 2016.

[62] Kevork N. Abazajian and Julian Heeck. Observing Dirac neutrinos in the cosmic microwave background. *Phys. Rev. D*, 100:075027, 2019.

[63] Yanou Cui, Lisa Randall, and Brian Shuve. A WIMPy Baryogenesis Miracle. *JHEP*, 04:075, 2012.

[64] John McDonald. Baryomorphosis: Relating the Baryon Asymmetry to the 'WIMP Miracle'. *Phys. Rev.*, D83:083509, 2011.

[65] Sacha Davidson and Martin Elmer. Similar Dark Matter and Baryon abundances with TeV-scale Leptogenesis. *JHEP*, 10:148, 2012.

[66] Yanou Cui and Raman Sundrum. Baryogenesis for weakly interacting massive particles. *Phys. Rev.*, D87(11):116013, 2013.

[67] Yanou Cui. A Review of WIMP Baryogenesis Mechanisms. *Mod. Phys. Lett.*, A30(37):1530028, 2015.

[68] Marco Farina, Angelo Monteux, and Chang Sub Shin. Twin mechanism for baryon and dark matter asymmetries. *Phys. Rev.*, D94(3):035017, 2016.

[69] J. Racker and N. Rius. Helicitogenesis: WIMPy baryogenesis with sterile neutrinos and other realizations. *JHEP*, 11:163, 2014.

[70] Yanou Cui. Natural Baryogenesis from Unnatural Supersymmetry. *JHEP*, 12:067, 2013.

[71] Yanou Cui and Brian Shuve. Probing Baryogenesis with Displaced Vertices at the LHC. *JHEP*, 02:049, 2015.

[72] Yanou Cui, Takemichi Okui, and Arash Yunesi. LHC Signatures of WIMP-triggered Baryogenesis. *Phys. Rev.*, D94(11):115022, 2016.

[73] The ATLAS collaboration. Search for long-lived, massive particles in events with a displaced vertex and a displaced muon in pp collisions at $\sqrt{s} = 13$ TeV with the ATLAS detector. 2019.

[74] Ryuichiro Kitano and Ian Low. Dark matter from baryon asymmetry. *Phys. Rev. D*, 71:023510, Jan 2005.

[75] Adam Falkowski, Joshua T. Ruderman, and Tomer Volansky. Asymmetric Dark Matter from Leptogenesis. *JHEP*, 05:106, 2011.

[76] Hooman Davoudiasl, David E. Morrissey, Kris Sigurdson, and Sean Tulin. Hylogenesis: A Unified Origin for Baryonic Visible Matter and Antibaryonic Dark Matter. *Phys. Rev. Lett.*, 105:211304, 2010.

[77] Kaustubh Agashe and Geraldine Servant. Baryon number in warped GUTs: Model building and (dark matter related) phenomenology. *JCAP*, 0502:002, 2005.

[78] Yanou Cui, Lisa Randall, and Brian Shuve. Emergent Dark Matter, Baryon, and Lepton Numbers. *JHEP*, 08:073, 2011.

[79] Nayara Fonseca, Lina Necib, and Jesse Thaler. Dark Matter, Shared Asymmetries, and Galactic Gamma Ray Signals. *JCAP*, 1602(02):052, 2016.

[80] Gilly Elor, Miguel Escudero, and Ann Nelson. Baryogenesis and Dark Matter from B Mesons. *Phys. Rev.*, D99(3):035031, 2019.

[81] Felix Kahlhoefer, Kai Schmidt-Hoberg, Thomas Schwetz, and Stefan Vogl. Implications of unitarity and gauge invariance for simplified dark matter models. *JHEP*, 02:016, 2016.

[82] Yanou Cui and Francesco D'Eramo. Surprises from complete vector portal theories: New insights into the dark sector and its interplay with Higgs physics. *Phys. Rev. D*, 96(9):095006, 2017.

[83] Michael L. Graesser, Ian M. Shoemaker, and Luca Vecchi. Asymmetric WIMP dark matter. *JHEP*, 10:110, 2011.

[84] Mu-Chun Chen. TASI 2006 Lectures on Leptogenesis. In *Proceedings of Theoretical Advanced Study Institute in Elementary Particle Physics : Exploring New Frontiers Using Colliders and Neutrinos (TASI 2006): Boulder, Colorado, June 4-30, 2006*, pages 123–176, 2007.

[85] Nicole F. Bell, Yi Cai, James B. Dent, Rebecca K. Leane, and Thomas J. Weiler. Enhancing Dark Matter Annihilation Rates with Dark Bremsstrahlung. *Phys. Rev. D*, 96(2):023011, 2017.

[86] James D. Wells. Annihilation cross-sections for relic densities in the low velocity limit. 1994.

[87] M. Garny, A. Hohenegger, and A. Kartavtsev. Medium corrections to the *cp*-violating parameter in leptogenesis. *Phys. Rev. D*, 81:085028, Apr 2010.

[88] Wolfram Research, Inc. Mathematica, Version 12.0, Champaign, IL, (2019).

[89] Matthew R. Buckley. Asymmetric dark matter and effective operators. *Phys. Rev. D*, 84:043510, Aug 2011.

[90] A. M. Sirunyan et al. Search for supersymmetry in proton-proton collisions at 13 TeV in final states with jets and missing transverse momentum. *Journal of High Energy Physics*, 2019(10), Oct 2019.

[91] Georges Aad et al. Search for direct production of electroweakinos in final states with one lepton, missing transverse momentum and a Higgs boson decaying into two b-jets in (pp) collisions at $\sqrt{s} = 13$ TeV with the ATLAS detector. 2019.

[92] Georges Aad et al. Search for electroweak production of charginos and sleptons decaying into final states with two leptons and missing transverse momentum in $\sqrt{s} = 13$ TeV pp collisions using the ATLAS detector. 2019.

[93] A. Abada et al. FCC-hh: The Hadron Collider. *Eur. Phys. J. ST*, 228(4):755–1107, 2019.

[94] N.V. Krasnikov. Influence of SU(2) x U(1) singlet scalars on Higgs boson signal at LHC. *Mod. Phys. Lett. A*, 13:893–898, 1998.

[95] Matthew Bowen, Yanou Cui, and James D. Wells. Narrow trans-TeV Higgs bosons and H —¿ hh decays: Two LHC search paths for a hidden sector Higgs boson. *JHEP*, 03:036, 2007.

[96] Luis A. Anchordoqui, Peter B. Denton, Haim Goldberg, Thomas C. Paul, Luiz H. M. da Silva, Brian J. Vlcek, and Thomas J. Weiler. Weinberg's higgs portal confronting recent lux and lhc results together with upper limits on B^+ and K^+ decay into invisibles. *Phys. Rev. D*, 89:083513, Apr 2014.

[97] David Curtin et al. Exotic decays of the 125 GeV Higgs boson. *Phys. Rev. D*, 90(7):075004, 2014.

[98] G. Belanger, F. Boudjema, A. Pukhov, and A. Semenov. Dark matter direct detection rate in a generic model with micrOMEGAs 2.2. *Comput. Phys. Commun.*, 180:747–767, 2009.

[99] Kyrylo Bondarenko, Alexey Boyarsky, Torsten Bringmann, Marco Hufnagel, Kai Schmidt-Hoberg, and Anastasia Sokolenko. Direct detection and complementary constraints for sub-GeV dark matter. 2019.

[100] C. E. Aalseth et al. DarkSide-20k: A 20 tonne two-phase LAr TPC for direct dark matter detection at LNGS. *Eur. Phys. J. Plus*, 133:131, 2018.

[101] Rouven Essig, Tomer Volansky, and Tien-Tien Yu. New Constraints and Prospects for sub-GeV Dark Matter Scattering off Electrons in Xenon. *Phys. Rev.*, D96(4):043017, 2017.

[102] D. S. Akerib et al. Projected WIMP Sensitivity of the LUX-ZEPLIN (LZ) Dark Matter Experiment. 2018.

[103] K. et. al. Abe. Search for proton decay via $p \to \nu K^+$ using 260 kiloton $\cdot$ year data of super-kamiokande. *Phys. Rev. D*, 90:072005, Oct 2014.

[104] Jost Migenda. The Hyper-Kamiokande Experiment: Overview & Status. In *Proceedings, Prospects in Neutrino Physics (NuPhys2016): London, UK, December 12-14, 2016*, 2017.

[105] R. Acciarri et al. Long-Baseline Neutrino Facility (LBNF) and Deep Underground Neutrino Experiment (DUNE). 2016.

[106] C. Abel et al. Measurement of the permanent electric dipole moment of the neutron. *Phys. Rev. Lett.*, 124(8):081803, 2020.

[107] V. Andreev et al. Improved limit on the electric dipole moment of the electron. *Nature*, 562(7727):355–360, 2018.

[108] Lotty Ackerman, Matthew R. Buckley, Sean M. Carroll, and Marc Kamionkowski. Dark Matter and Dark Radiation. pages 277–286, 10 2008.

[109] Jonathan L. Feng, Huitzu Tu, and Hai-Bo Yu. Thermal Relics in Hidden Sectors. *JCAP*, 10:043, 2008.

[110] Xiaoyong Chu, Thomas Hambye, and Michel H.G. Tytgat. The Four Basic Ways of Creating Dark Matter Through a Portal. *JCAP*, 05:034, 2012.

[111] Maxim Pospelov, Adam Ritz, and Mikhail Voloshin. Secluded wimp dark matter. *Physics Letters B*, 662(1):53–61, Apr 2008.

[112] Michael J. Baker, Joachim Brod, Sonia El Hedri, Anna Kaminska, Joachim Kopp, Jia Liu, Andrea Thamm, Maikel de Vries, Xiao-Ping Wang, Felix Yu, and et al. The coannihilation codex. *Journal of High Energy Physics*, 2015(12):1–86, Dec 2015.

[113] Jeff Asaf Dror, Eric Kuflik, and Wee Hao Ng. Codecaying dark matter. *Physical Review Letters*, 117(21), Nov 2016.

[114] B. Pontecorvo. Mesonium and anti-mesonium. *Sov. Phys. JETP*, 6:429, 1957. [Zh. Eksp. Teor. Fiz.33,549(1957)].

[115] B. Pontecorvo. Neutrino Experiments and the Problem of Conservation of Leptonic Charge. *Sov. Phys. JETP*, 26:984–988, 1968. [Zh. Eksp. Teor. Fiz.53,1717(1967)].

[116] Ziro Maki, Masami Nakagawa, and Shoichi Sakata. Remarks on the unified model of elementary particles. *Prog. Theor. Phys.*, 28:870–880, 1962.

[117] Q.R. Ahmad et al. Measurement of the rate of $\nu_e + d \rightarrow p + p + e^-$ interactions produced by ^8B solar neutrinos at the Sudbury Neutrino Observatory. *Phys. Rev. Lett.*, 87:071301, 2001.

[118] Steven Weinberg. A Model of Leptons. *Phys. Rev. Lett.*, 19:1264–1266, 1967.

[119] Steven Weinberg. Baryon and Lepton Nonconserving Processes. *Phys.Rev.Lett.*, 43:1566–1570, 1979.

[120] M. Tanabashi et al. Review of Particle Physics: 14. Neutrino Masses, Mixings, and Oscillations. *Phys. Rev. D*, 98(3):030001, 2018.

[121] Lincoln Wolfenstein. Different Varieties of Massive Dirac Neutrinos. *Nucl. Phys. B*, 186:147–152, 1981.

[122] Darwin Chang and Otto C. W. Kong. Pseudo-Dirac neutrinos. *Phys. Lett. B*, 477:416–423, 2000.

[123] K. R. S. Balaji, Anna Kalliomaki, and Jukka Maalampi. Revisiting pseudoDirac neutrinos. *Phys. Lett. B*, 524:153–160, 2002.

[124] André de Gouvêa, Wei-Chih Huang, and James Jenkins. Pseudo-dirac neutrinos in the new standard model. *Phys. Rev. D*, 80:073007, Oct 2009.

[125] S. L. Shapiro, S. A. Teukolsky, and I. Wasserman. DO NEUTRINO REST MASSES AFFECT COSMOLOGICAL HELIUM PRODUCTION? *Phys. Rev. Lett.*, 45:669–672, 1980.

[126] Edward W. Kolb and Robert J. Scherrer. Massive Neutrinos and Primordial Nucleosynthesis. *Phys. Rev.*, D25:1481, 1982.

[127] Nicholas DePorzio, Weishuang Linda Xu, Julian B. Muñoz, and Cora Dvorkin. Finding eV-scale Light Relics with Cosmological Observables. 6 2020.

[128] Karin Dick, Manfred Lindner, Michael Ratz, and David Wright. Leptogenesis with Dirac neutrinos. *Phys. Rev. Lett.*, 84:4039–4042, 2000.

[129] Hitoshi Murayama and Aaron Pierce. Realistic Dirac leptogenesis. *Phys. Rev. Lett.*, 89:271601, 2002.

[130] Pei-Hong Gu and Hong-Jian He. Neutrino Mass and Baryon Asymmetry from Dirac Seesaw. *JCAP*, 12:010, 2006.

[131] Pei-Hong Gu. From Dirac neutrino masses to baryonic and dark matter asymmetries. *Nucl. Phys. B*, 872:38–61, 2013.

[132] Julian Heeck. Leptogenesis with Lepton-Number-Violating Dirac Neutrinos. *Phys. Rev. D*, 88:076004, 2013.

[133] Steven Abel and Veronique Page. (Pseudo)-Dirac neutrinos and leptogenesis. *AIP Conf. Proc.*, 878(1):341–346, 2006.

[134] Y. H. Ahn, Sin Kyu Kang, and C. S. Kim. A Model for Pseudo-Dirac Neutrinos: Leptogenesis and Ultra-High Energy Neutrinos. *JHEP*, 10:092, 2016.

[135] Vernon Barger, Paul Langacker, and Hye-Sung Lee. Primordial nucleosynthesis constraints on Z' properties. *Phys. Rev. D*, 67:075009, 2003.

[136] Luis Alfredo Anchordoqui and Haim Goldberg. Neutrino cosmology after WMAP 7-Year data and LHC first Z' bounds. *Phys. Rev. Lett.*, 108:081805, 2012.

[137] Luis A. Anchordoqui, Haim Goldberg, and Gary Steigman. Right-Handed Neutrinos as the Dark Radiation: Status and Forecasts for the LHC. *Phys. Lett. B*, 718:1162–1165, 2013.

[138] A. Solaguren-Beascoa and M.C. Gonzalez-Garcia. Dark Radiation Confronting LHC in Z' Models. *Phys. Lett. B*, 719:121–125, 2013.

[139] Dibyendu Nanda and Debasish Borah. Connecting light dirac neutrinos to a multi-component dark matter scenario in gauged

$$b - l$$

model. *The European Physical Journal C*, 80(6), Jun 2020.

[140] Tom Banks and Nathan Seiberg. Symmetries and Strings in Field Theory and Gravity. *Phys. Rev. D*, 83:084019, 2011.

[141] James Alvey and Miguel Escudero. The axion quality problem: Global symmetry breaking and wormholes, 2020.

[142] Lawrence J. Hall, Karsten Jedamzik, John March-Russell, and Stephen M. West. Freeze-In Production of FIMP Dark Matter. *JHEP*, 03:080, 2010.

[143] Scott Dodelson and Lawrence M. Widrow. Sterile-neutrinos as dark matter. *Phys. Rev. Lett.*, 72:17–20, 1994.

[144] Shainen M. Davidson and Heather E. Logan. Dirac neutrinos from a second Higgs doublet. *Phys. Rev. D*, 80:095008, 2009.

[145] Ernest Ma and Oleg Popov. Pathways to Naturally Small Dirac Neutrino Masses. *Phys. Lett. B*, 764:142–144, 2017.

[146] Chang-Yuan Yao and Gui-Jun Ding. Systematic analysis of Dirac neutrino masses from a dimension five operator. *Phys. Rev. D*, 97(9):095042, 2018.

[147] Pavel Fileviez Pérez, Clara Murgui, and Alexis D. Plascencia. Neutrino-dark matter connections in gauge theories. *Phys. Rev. D*, 100:035041, Aug 2019.

[148] Chengcheng Han, M. L. López-Ibáñez, Bo Peng, and Jin Min Yang. Dirac dark matter in $u(1)_{B-L}$ with stueckelberg mechanism, 2020.

[149] K. Assamagan et al. Upper limit of the muon-neutrino mass and charged pion mass from momentum analysis of a surface muon beam. *Phys. Rev. D*, 53:6065–6077, 1996.

[150] M. et al Athanas. Limit on the tau neutrino mass from $\tau^- \to \pi^-\pi^+\pi^-\pi^0\nu_\tau$. *Phys. Rev. D*, 61:052002, Feb 2000.

[151] Jong-Mann Yang, David N. Schramm, Gary Steigman, and Robert T. Rood. Constraints on Cosmology and Neutrino Physics from Big Bang Nucleosynthesis. *Astrophys. J.*, 227:697–704, 1979.

[152] Zhen Hou, Ryan Keisler, Lloyd Knox, Marius Millea, and Christian Reichardt. How Massless Neutrinos Affect the Cosmic Microwave Background Damping Tail. *Phys.Rev.*, D87:083008, 2013.

[153] Sergei Bashinsky and Uros Seljak. Neutrino perturbations in CMB anisotropy and matter clustering. *Phys. Rev.*, D69:083002, 2004.

[154] Brent Follin, Lloyd Knox, Marius Millea, and Zhen Pan. First Detection of the Acoustic Oscillation Phase Shift Expected from the Cosmic Neutrino Background. *Phys. Rev. Lett.*, 115(9):091301, 2015.

[155] Daniel Baumann, Daniel Green, Joel Meyers, and Benjamin Wallisch. Phases of New Physics in the CMB. *JCAP*, 01:007, 2016.

[156] Christopher Brust, Yanou Cui, and Kris Sigurdson. Cosmological Constraints on Interacting Light Particles. *JCAP*, 08:020, 2017.

[157] Kevork N. Abazajian et al. CMB-S4 Science Book, First Edition. 10 2016.

[158] Kevork Abazajian et al. CMB-S4 Science Case, Reference Design, and Project Plan. 7 2019.

[159] A.D. Dolgov. Cosmology and Neutrino Properties. *Phys.Atom.Nucl.*, 71:2152–2164, 2008.

[160] Sunny Vagnozzi, Elena Giusarma, Olga Mena, Katherine Freese, Martina Gerbino, Shirley Ho, and Massimiliano Lattanzi. Unveiling ν secrets with cosmological data: neutrino masses and mass hierarchy. *Phys. Rev. D*, 96(12):123503, 2017.

[161] Edward W. Kolb and Michael Stanley Turner. *The Early Universe*. Westview Press, 1990.

[162] S. Betts et al. Development of a Relic Neutrino Detection Experiment at PTOLEMY: Princeton Tritium Observatory for Light, Early-Universe, Massive-Neutrino Yield. In *Community Summer Study 2013: Snowmass on the Mississippi*, 7 2013.

[163] E. Baracchini et al. PTOLEMY: A Proposal for Thermal Relic Detection of Massive Neutrinos and Directional Detection of MeV Dark Matter. 8 2018.

[164] Andrew J. Long, Cecilia Lunardini, and Eray Sabancilar. Detecting non-relativistic cosmic neutrinos by capture on tritium: phenomenology and physics potential. *JCAP*, 08:038, 2014.

[165] M.G. Betti et al. Neutrino physics with the PTOLEMY project: active neutrino properties and the light sterile case. *JCAP*, 07:047, 2019.

[166] Raffaele Tito D'Agnolo and Joshua T. Ruderman. Light dark matter from forbidden channels. *Phys. Rev. Lett.*, 115:061301, Aug 2015.

[167] Kim Griest and David Seckel. Three exceptions in the calculation of relic abundances. *Phys. Rev. D*, 43:3191–3203, 1991.

[168] W. Buchmuller, R. D. Peccei, and T. Yanagida. Leptogenesis as the origin of matter. *Ann. Rev. Nucl. Part. Sci.*, 55:311–355, 2005.

Appendix A

Relating Baryon and Lepton Asymmetries for WIMP Cogenesis before Electroweak Phase Transition

In this Appendix we derive the relation between baryon and lepton asymmetries for WIMP cogenesis before electroweak phase transition. We will follow the general procedure laid out for the SM [20, 84, 168], while adding in the effects from new particles in WIMP cogenesis models.

A.1 WIMP Decay to Baryons and ADM (Sec. 2.2)

Before the electroweak phase transition (EWPT), chemical equilibrium of SM left-handed and right-handed quarks and leptons, Higgs bosons, and new fields introduced by WIMP cogenesis ϕ, ψ, and χ determines the relationship between number densities of baryons, leptons, and ADM candidate χ. This relationship and the observed ratio $\Omega_\chi/\Omega_B \approx 5$ determines the ADM mass as in Eq. 2.1. In the high temperature plasma of the early universe the quarks, leptons, Higgs, ϕ, ψ, and χ interact via gauge, Yukawa, and sphaleron processes. The interactions that constrain the chemical potentials in thermal equilibrium are:

1. The effective sphaleron interaction $\mathcal{O}_{\rm sph} \sim \prod_i (Q_i Q_i Q_i L_i)$ gives rise to

$$\sum_i (3\mu_{Q_i} + \mu_{L_i}) = 0 \tag{A.1}$$

   where i is an index counting the number of generations of fermions and Q_i are the LH quarks and L_i are the LH leptons.

2. The $SU(3)$ QCD instanton processes lead to interactions between LH quarks and RH quarks u_i and d_i. These interactions are described by $\mathcal{O}_{\rm inst} \sim \prod_i (Q_i Q_i u_i^c d_i^c)$ which leads to

$$\sum_i (2\mu_{Q_i} - \mu_{u_i} - \mu_{d_i}) = 0 \tag{A.2}$$

3. The total hypercharge of the plasma must vanish at all temperatures. In addition to the hypercharge carried by SM states, ϕ and ψ also contribute, while the magnitude of the contribution depends on their masses relative to EWPT temperature $T_{\rm EWPT}$. Non-relativistic ϕ and ψ bear a Boltzmann suppression in their equilibrium density

distribution which makes their contribution to hypercharge density negligible relative to relativistic species. Given the unknowns around determining $T_{\rm EWPT}$ and the wide ranges $m_\psi \sim m_\phi$, we consider possibilities at two limits: $m_\psi \sim m_\phi \ll T_{\rm EWPT}$ and $m_\psi \sim m_\phi \gg T_{\rm EWPT}$. With $m_\psi \sim m_\phi \ll T_{\rm EWPT}$, we have:

$$\sum_i (\mu_{Q_i} + 2\mu_{u_i} - \mu_{d_i} - \mu_{L_i} - \mu_{e_i} + \frac{2N_H}{N_f}\mu_H + \mu_{\phi_i} + \mu_{\psi_i}) = 0 \tag{A.3}$$

where N_H is the number of Higgs bosons (1 in the SM) and N_f is the number of generations of fermions. With $m_\psi \sim m_\phi \gg T_{\rm EWPT}$, we have:

$$\sum_i (\mu_{Q_i} + 2\mu_{u_i} - \mu_{d_i} - \mu_{L_i} - \mu_{e_i} + \frac{2N_H}{N_f}\mu_H) = 0 \tag{A.4}$$

4. The Yukawa interactions of the SM $\mathcal{O}_{\rm SM} \sim \bar{Q}_i H d_j,\ \bar{Q}_i \tilde{H} u_j,\ \bar{L}_i H e_j$ and the Yukawa interactions introduced in Sec 2.2.1 $\mathcal{O}_{\rm WIMP} \sim \phi_i \bar{d}_i \chi^c,\ \beta_{ijk}\phi_i \bar{\psi}_j u_k$, while in equilibrium give rise to

$$\begin{aligned} \mu_{Q_i} - \mu_H - \mu_{d_j} &= 0 \\ \mu_{Q_i} + \mu_H - \mu_{u_j} &= 0 \\ \mu_{L_i} - \mu_H - \mu_{e_j} &= 0 \\ \mu_{d_i} - \mu_{\phi_i} + \mu_\chi &= 0 \\ \mu_{\psi_j} - \mu_{\phi_i} - \mu_{u_k} &= 0 \end{aligned} \tag{A.5}$$

Since the temperature before the EWPT is much greater than the masses of the quarks, leptons, and χ we take the massless limit where their number densities are $n_i - \bar{n}_i = \frac{1}{6} g \mu_i T^2$. The baryon, lepton, and χ number densities are $n_B = \frac{1}{6} B T^2$, $n_L = \frac{1}{6} L T^2$, and $n_X = \frac{1}{6} X T^2$,

respectively, where

$$B = \sum_i (2\mu_{Q_i} + \mu_{u_i} + \mu_{d_i}) \tag{A.6}$$

$$L = \sum_i (2\mu_{L_i} + \mu_{e_i}) \tag{A.7}$$

$$X = \mu_\chi \tag{A.8}$$

With SM alone, the combination of asymmetry $B - L$ is preserved, while in our model $B - L + 2X$ would be preserved. Assuming equilibrium amongst the various generations $\mu_{Q_i} \equiv \mu_Q$, $\mu_{L_i} \equiv \mu_L$, $\mu_{e_i} \equiv \mu_e$, $\mu_{q_i} \equiv \mu_q$, $\mu_{\phi_i} \equiv \mu_\phi$, $\mu_{\psi_i} \equiv \mu_\psi$ allows us to write $B = N_f(2\mu_Q + \mu_u + \mu_d)$, $L = N_f(2\mu_L + \mu_e)$. Thus the preserved combination, per generation, is

$$\left[2\mu_Q + \mu_u + \mu_d - (2\mu_L + \mu_e)\right] + 2\mu_\chi = 0 \tag{A.9}$$

Let us first analyze the case of $m_\psi \sim m_\phi \ll T_{\rm EWPT}$. Using the Yukawa interactions of Eqs. A.5 , Eq. A.9 can be recast as $\mu_\chi = -\frac{1}{2}(B-L) = -\frac{1}{2}(13\mu_Q + \mu_H) = \mu_\phi - \mu_Q + \mu_H$. The effective sphaleron interactions of Eq. A.1 give $\mu_L = -3\mu_Q$. Substituting this and Eqs. A.5 in Eq. A.3 allows us to solve μ_H in terms of μ_Q which allows us to write all chemical potentials in terms of μ_Q using Eqs. A.5:

$$\begin{aligned}
\mu_L &= -3\mu_Q & \mu_H &= \frac{N_f}{N_f + N_H}\mu_Q \\
\mu_u &= \frac{2Nf + N_H}{N_f + N_H}\mu_Q & \mu_d &= \frac{N_H}{N_f + N_H}\mu_Q \\
\mu_e &= -\frac{4N_f + 3N_H}{N_f + N_H}\mu_Q & \mu_\phi &= -\frac{1}{2}\left(\frac{14N_f + 11N_H}{N_f + N_H}\right)\mu_Q \\
\mu_\psi &= -\frac{1}{2}\left(\frac{10N_f + 9N_H}{N_f + N_H}\right)\mu_Q & \mu_\chi &= -\frac{1}{2}\left(\frac{14N_f + 13N_H}{N_f + N_H}\right)\mu_Q
\end{aligned} \tag{A.10}$$

Plugging these into the equations for B, L and $B-L$ allows us to write the relations between them:

$$B = 4N_f\mu_Q \tag{A.11}$$

$$L = -\frac{10N_f+9N_H}{N_f+N_H}N_f\mu_Q \tag{A.12}$$

$$B-L = \frac{14N_f+13N_H}{N_f+N_H}N_f\mu_Q \equiv c_s^{-1}B \tag{A.13}$$

where

$$c_s \equiv B/(B-L) = \frac{4(N_f+N_H)}{14N_f+13N_H} \tag{A.14}$$

In the other limit, $m_\psi \sim m_\phi \gg T_{\rm EWPT}$, we use Eq. A.4. In this case, we need only use the SM Yukawa interactions to find the SM chemical potentials (and thus $c_s \equiv B/B-L$). We can still use Eq. A.9 to find the chemical potentials of ϕ, ψ, and χ in terms of μ_Q:

$$\begin{aligned}
&\mu_L = -3\mu_Q && \mu_H = -\frac{4N_f}{2N_f+N_H}\mu_Q \\
&\mu_u = -\frac{2N_f-N_H}{2N_f+N_H}\mu_Q && \mu_d = \frac{6N_f+N_H}{2N_f+N_H}\mu_Q \\
&\mu_e = -\frac{2N_f+3N_H}{2N_f+N_H}\mu_Q && \mu_\phi = -\frac{1}{2}\left(\frac{10N_f+11N_H}{2N_f+N_H}\right)\mu_Q \\
&\mu_\psi = -\frac{1}{2}\left(\frac{14N_f+9N_H}{2N_f+N_H}\right)\mu_Q && \mu_\chi = -\frac{1}{2}\left(\frac{22N_f+13N_H}{2N_f+N_H}\right)\mu_Q
\end{aligned} \tag{A.15}$$

Plugging these into the same equations for B, L, and $B-L$ yields

$$B = 4N_f\mu_Q \tag{A.16}$$

$$L = -\frac{14N_f+9N_H}{2N_f+N_H}N_f\mu_Q \tag{A.17}$$

$$B-L = \frac{22N_f+13N_H}{2N_f+N_H}N_f\mu_Q \equiv c_s^{-1}B \tag{A.18}$$

which gives the same result as that found in the SM [84]

$$c_s \equiv B/(B-L) = \frac{8N_f+4N_H}{22N_f+13N_H} \tag{A.19}$$

A.2 WIMP Decay to Leptons and ADM (Sec. 2.3)

In the model outlined in Sec. 2.3 WIMP cogenesis, the biggest change is to the Yukawa interactions: $\mathcal{O}_{\rm WIMP} \sim \phi \bar{L} \chi^c,\ H \bar{\psi} \chi$ which changes the last two Yukawa interactions in Eqs. A.5 in a straightforward fashion. We note also the mass of the ADM candidate χ is fixed by the observed ratio of DM to baryon energy densities fixed by:

$$\Omega_{DM} \ = \ \frac{2 m_\chi s_0}{\rho_0} \epsilon_1 Y_{Y_1, f.o.} \ = \ 5 \Omega_B \ = \ \frac{5 c_s s_0 m_n}{|c_s - 1| \rho_0} \epsilon_1 Y_{Y_1, f.o.} \quad \Longrightarrow \quad m_\chi \ = \ \frac{5 c_s}{2|c_s - 1|} m_n$$

Following the same procedure, we find the chemical potentials in terms of μ_Q to be

$$\begin{aligned}
\mu_L &= -3\mu_Q & \mu_H &= \frac{4N_f}{2N_f + N_H}\mu_Q \\
\mu_d &= -\frac{2N_f - N_H}{2N_f + N_H}\mu_Q & \mu_u &= \frac{6N_f + N_H}{2N_f + N_H}\mu_Q \\
\mu_e &= -\frac{10N_f + 3N_H}{2N_f + N_H}\mu_Q & \mu_\phi &= -\frac{1}{2}\left(\frac{42N_f + 19N_H}{2N_f + N_H}\right)\mu_Q \\
\mu_\chi &= -\frac{1}{2}\left(\frac{30N_f + 13N_H}{2N_f + N_H}\right)\mu_Q & \mu_\psi &= -\frac{1}{2}\left(\frac{22N_f + 13N_H}{2N_f + N_H}\right)\mu_Q
\end{aligned} \tag{A.20}$$

Again, following the same procedure as before we find

$$B \ = \ 4N_f \mu_Q \tag{A.21}$$

$$L \ = \ -\frac{22N_f + 9N_H}{2N_f + N_H} N_f \mu_Q \tag{A.22}$$

$$B - L \ = \ \frac{30N_f + 13N_H}{2N_f + N_H} N_f \mu_Q \equiv c_s^{-1} B \tag{A.23}$$

where

$$c_s \equiv \frac{B}{B - L} = \frac{8N_f + 4N_H}{30N_f + 13N_H} \tag{A.24}$$

In the case that ϕ and ψ are heavy, the same result as that given in Eq. A.19 is found, but the chemical potentials of ϕ, ψ and χ are

$$\mu_\phi = -\frac{1}{2}\left(\frac{34N_f + 19N_H}{2N_f + N_H}\right)$$
$$\mu_\psi = -\frac{1}{2}\left(\frac{30N_f + 13N_H}{2N_f + N_H}\right)$$
$$\mu_\chi = -\frac{1}{2}\left(\frac{22N_f + 13N_H}{2N_f + N_H}\right).$$